Supplementary data for article:

Božić, A. R.; Filipović, N. R.; Verbić, T.; Milčić, M. K.; Todorović, T.; Cvijetić, I.; Klisurić, O. R.; Radišić, M. M.; Marinković, A. D. A Detailed Experimental and Computational Study of Monocarbohydrazones. *Arabian Journal of Chemistry* **2017**. https://doi.org/10.1016/j.arabjc.2017.08.010

A detailed experimental and computational study of monocarbohydrazones

Aleksandra R. Božić[a]*, Nenad R. Filipović*[b]*, Tatjana Ž. Verbić*[c]*, Miloš K. Milčić*[c]*, Tamara R. Todorović*[c]*, Ilija N. Cvijetić*[d]*, Olivera R. Klisurić*[e]*, Marina Radišić*[f]*, Aleksandar D. Marinković*[f]

[a]*Belgrade Polytechnic, Brankova 17, 11000 Belgrade, Serbia,*
[b]*Faculty of Agriculture, University of Belgrade, Nemanjina 6, Belgrade, Serbia,*
[c]*Faculty of Chemistry, University of Belgrade, Studentski trg 12-16, 11000 Belgrade, Serbia*
[d]*Innovation Center of the Faculty of Chemistry, University of Belgrade, Studentski Trg 16, 11000 Belgrade, Serbia*
[e]*Department of Physics, Faculty of Sciences, University of Novi Sad, Novi Sad, Serbia*
[f]*Faculty of Technology and Metallurgy, University of Belgrade, Karnegijeva 4, Belgrade, Serbia*

2. Experimental

2.1 Materials

All reagents of p.a. quallity: benzaldehyde, salicylaldehyde, 2-pyridinecarboxaldehyde, 3-pyridinecarboxaldehyde, 4-pyridinecarboxaldehyde, methyl phenyl ketone, methyl 2-pyridyl ketone, methyl 3-pyridyl ketone, methyl 4-pyridyl ketone, 2-quinolinecarboxaldehyde, and carbohydrazide (dhO) were obtained from Sigma. 8-Quinolinecarboxaldehyde (98 %) and 8-hydroxy-2-quinolinecarboxaldehyde (98 %) were obtained from Acros Organics. All used solvents were of spectroscopic quality (Sigma).

2.2. Synthesis of monocarbohydrazones

Table S1. Numbering of atoms in monocarbohydrazones **1-12** used in NMR.

1	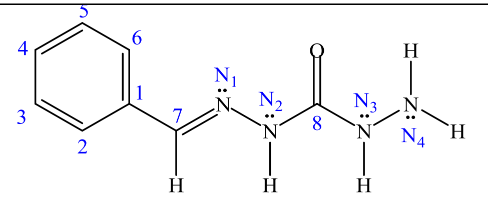	**5**	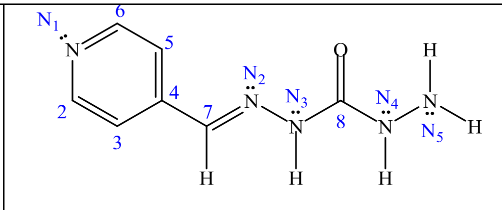	**9**	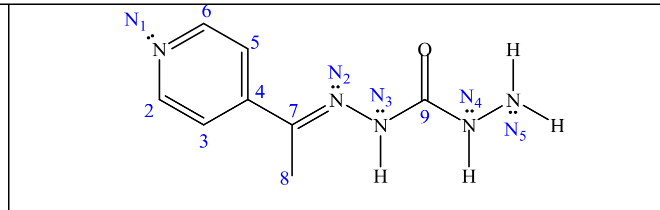
2	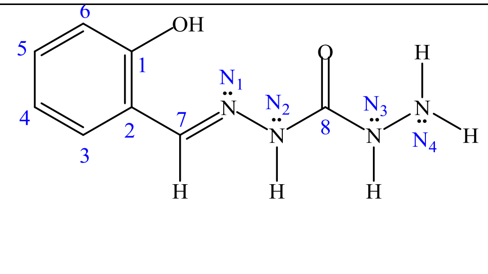	**6**	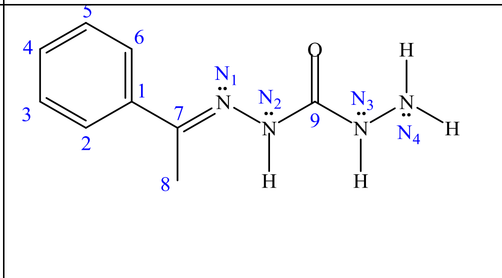	**10**	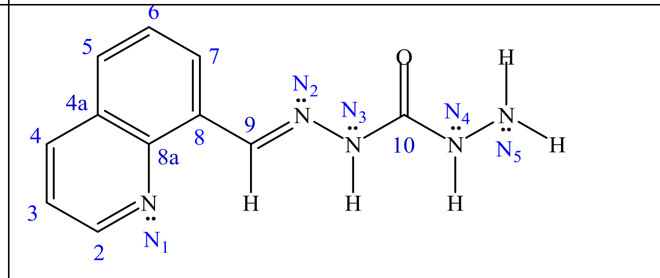
3	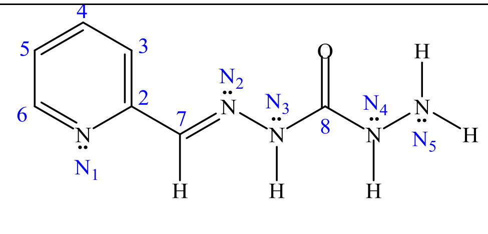	**7**	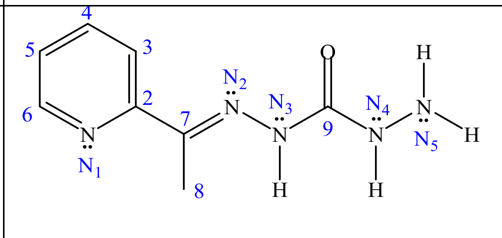	**11**	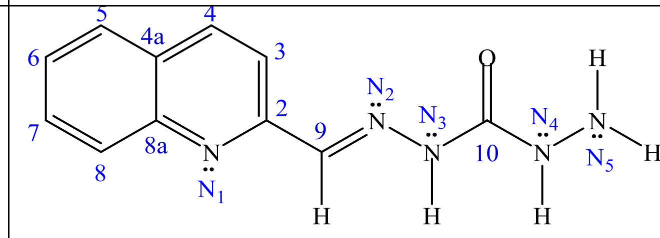
4	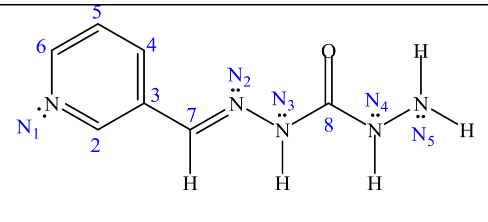	**8**	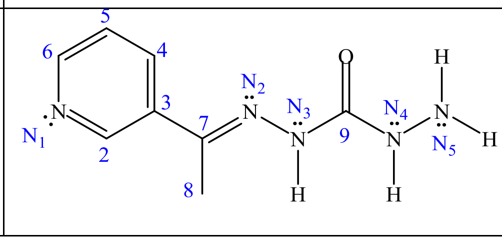	**12**	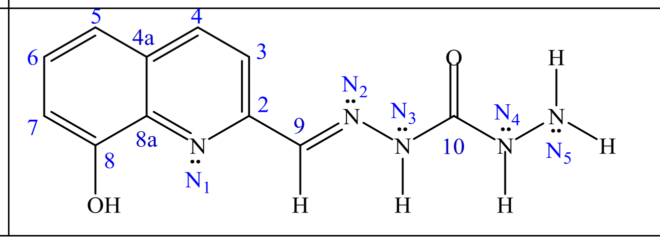

2.3. Methods

Table S2. Solvent parameters (Kamlet et al., 1983; Marcus, 1993) used in Kamlet–Taft equation.

	Solvent[a]	π^*	β	α
1	Ethanol (EtOH)	0.54	0.75	0.86
2	Methanol (MeOH)	0.6	0.66	0.98
3	1-Propanol (1-PrOH)	0.52	0.90	0.84
4	1-Butanol (1-BuOH)	0.47	0.88	0.79
5	2-Methylpropan-1-ol (*i*-BuOH)	0.4	0.84	0.79
6	1-Penthanol (1-PeOH)	0.4	0.86	0.84
7	3-Methylbutan-1-ol (*i*-PeOH)	0.4	0.86	0.84
8	2-Metoxyethanol (2ME)	0.71	0	0
9	2-Chloroethanol (2CE)	0.46	0.53	1.28
10	Water	1.09	0.47	1.17
11	Acetonitrile (AcN)	0.75	0.40	0.19
12	Chloroform (Chl)	0.58	0	0.44
13	Diethyl ether (Et_2O)	0.27	0.47	0
14	Tetrahydrofuran (THF)	0.58	0.55	0
15	Dioxane	0.55	0.37	0
16	2-Pyrrolodinone (2-Py)	0.85	0.77	0.36
17	Ethyl Acetate (EtAc)	0.55	0.45	0
18	Dichlormethane (DCM)	0.82	0.1	0.13
19	1-Methyl-2-pyrrolidinone (NMP)	0.92	0.77	0
20	*N*,*N*-Dimethylformamide (DMF)	0.88	0.69	0
21	Dimethyl sulfoxide (DMSO)	1	0.76	0
22	*N*,*N*-Dimethylacetamide (DMA)	0.88	0.76	0

[a]Solvent abbreviation was taken from www.chemnetbase

Table S3. Solvent parameters , 2009) used in Catalán equation[a].

	Solvent	*SP*	*SdP*	*SA*	*SB*
1	Ethanol (EtOH)	0.608	0.904	0.605	0.545
2	Methanol (MeOH)	0.633	0.783	0.4	0.658
3	1-Propanol (1-PrOH)	0.658	0.748	0.367	0.782
4	1-Butanol (1-BuOH)	0.674	0.655	0.341	0.809
5	2-Methylpropan-1-ol (*i*-BuOH)	0.656	0.706	0.221	0.888
6	1-Penthanol (1-PeOH)	0.687	0.587	0.319	0.86
7	3-Methylbutan-1-ol (*i*-PeOH)	0,667	0,665	0,204	0,916
8	2-Metoxyethanol (2ME)	0.7704	0.9736	0.56	0.38
9	2-Chloroethanol (2CE)	0.6996	0.8952	0.36	0.56
10	Water (H_2O)	0.681	0.997	1.062	0.025
11	Acetonitrile (AcN)	0.645	0.974	0.044	0.286
12	Chloroform (Chl)	0.783	0.614	0.047	0.071
13	Diethyl ether (Et_2O)	0.617	0.385	0	0.562
14	Teterahydrofuran (THF)	0.714	0.634	0	0.591
15	Dioxane	0.737	0.312	0	0.444
16	Ethyl Acetate (EtAc)	0.83	1	0.072	0.647
17	Dichlormethane (DCM)	0.814	1.006	0.549	0.414
18	1-Methyl-2-pyrrolidinone (NMP)	0.656	0.603	0	0.542
19	*N*,*N*-Dimethylformamide (DMF)	0.761	0.769	0.04	0.178
20	Dimethyl sulfoxide (DMSO)	0.812	0.959	0.024	0.613
21	*N*,*N*-Dimethylacetamide (DMA)	0.759	0.977	0.031	0.613

[a] Catalán parameters for 2-Pyrrolodinone are not available

Table S4. Hammett substituent parameters (Chapman and Shorter, 1978; Hansch et al., 1995).

	R_1	R_2	σ	σ_{pH+}
1	Phenyl	H	-0.01	
2	2-Hydroxyphenyl	H	-0.09	-0.09
3	2-Pyridyl	H	0.73	0.88
4	3-Pyridyl	H	0.55	1.82
5	4-Pyridyl	H	0.8	2.42
6	Phenyl	Me	0.036	
7	2-Pyridyl	Me	0.776	0.926
8	3-Pyridyl	Me	0.596	1.866
9	4-Pyridyl	Me	0.846	2.466
10	8-Quinolyl	H	0.07	
11	2-Quinolyl	H	1.3	
12	8-Hydroxy-2-Quinolyl	H	0.57	
l1	2-Thienyl (Okawara et al., 2006)	H	0.71	
l2	4-Metoxyphenyl (Okawara et al., 2006)	H	-0.27	
l3	4-Carboxyphenyl (Okawara et al., 2006)	H	0.45	
l4	4-Hydroxyphenyl (Okawara et al., 2006)	H	-0.37	

3. Results and discussion

3.1 Synthesis and compound characterization

*Spectral data for compounds **1-12***

Benzaldehyde carbohydrazone (**1**). White solid was recrystallized from absolute methanol. Yield: 85%. M.p. 165-166°C (lit. M.p. 169-170). Elemental analysis calcd. for $C_8H_{10}N_4O$ (Mw = 178.09 g mol^{-1}): C, 53.92; H, 5.66; N, 31.44%; Found: C, 53.12; H, 5.77; N, 31.23%. IR (KBr, cm^{-1}) ν_{max}: 3280s (NH_2), 3071s (NH), 1678vs (C=O), 1600m (C=N). ^{1}H NMR (100 MHz, DMSO-d_6,) δ (ppm): 4.10 (s, 2H, H2–N4); 7.55-7.80 (m, 5H, H–C2-C6); 7.92 (s, 1H, H–C7); 8.10 (s, 1H, H–N3); 10.50 (s. 1H, H-N2). ^{13}C NMR (126 MHz, DMSO-d_6, δ (ppm): 125.49 (C3=C5); 128.68 (C2=C6); 131.61 (C4); 134.85 (C1); 140.76 (C7); 157.20 (C8).

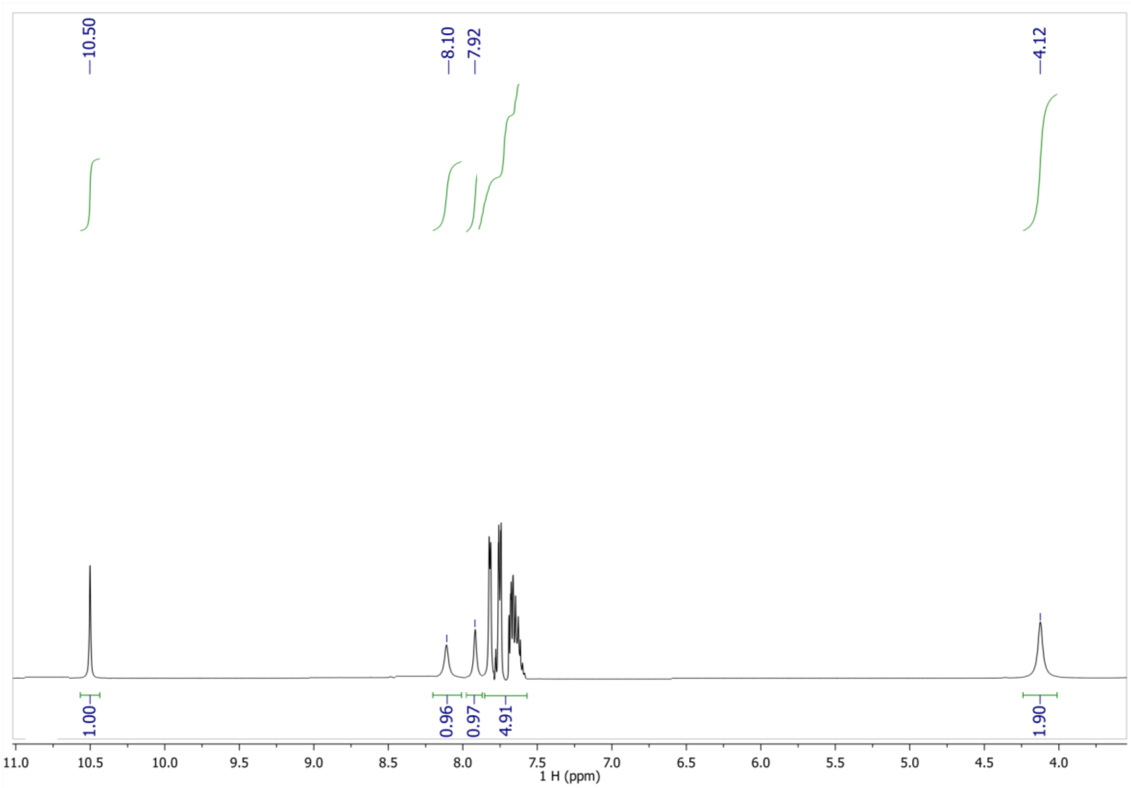

Figure S1. ^{1}H NMR spectrum of **1** in DMSO-d_6.

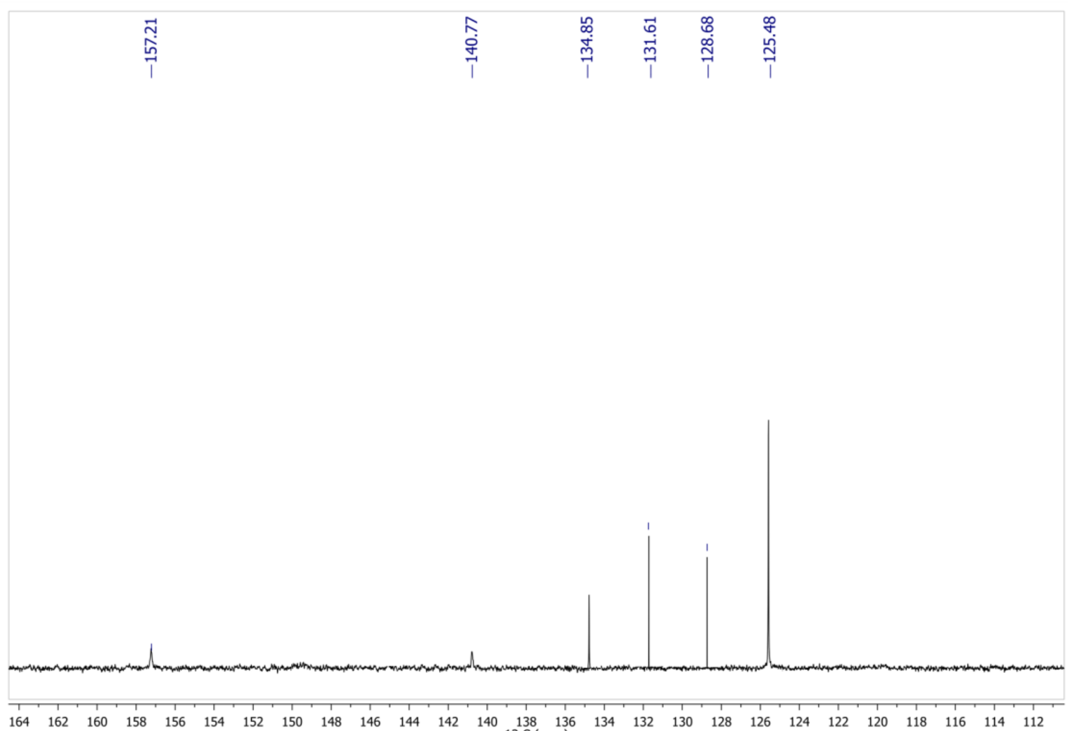

Figure S2. ^{13}C NMR spectrum of **1** in DMSO-d_6.

Salycilaldehide carbohydrazone (**2**). White solid was recrystallized from absolute methanol. Yield: 66%. M.p. 180-181°C (lit. M.p. no data). Elemental analysis calcd. for $C_8H_9N_4O_2$ (Mw = 245.24 g mol^{-1}): C, 49.74; H, 4.70; N, 29.00%; Found: C, 49.68; H, 4.66; N, 28.93%. IR (KBr, cm^{-1}) ν_{max}: 3353s (OH), 3282s (NH_2), 3096s (NH), 1680vs (C=O), 1640m (C=N). literature data: ^{1}H NMR (500 MHz, DMSO-d_6, δ / ppm): 4.16 (s, 2H, H2–N4), 6.71-6.91 (m, 2H, H–C5, H-C3), 7.18 (dd, 1H, H–C4, $^3J_{4,3}$ = 7.7 Hz, $^3J_{4,5}$ =1.8 Hz), 7.64 (s, 1H, H–C6), 7.92 (s, 1H, H–N3), 8.20 (1H, H–C7), 10.40 (br.s. 2H, OH, H–N2). ^{13}C NMR (90 MHz, DMSO-*d*6, δ / ppm): 116.09 (C3), 119.22 (C5), 120.06 (C2), 127.86 (C6), 130.23 (C4), 140.04 (C7), 156.24 (C1), 157.30 (C8).

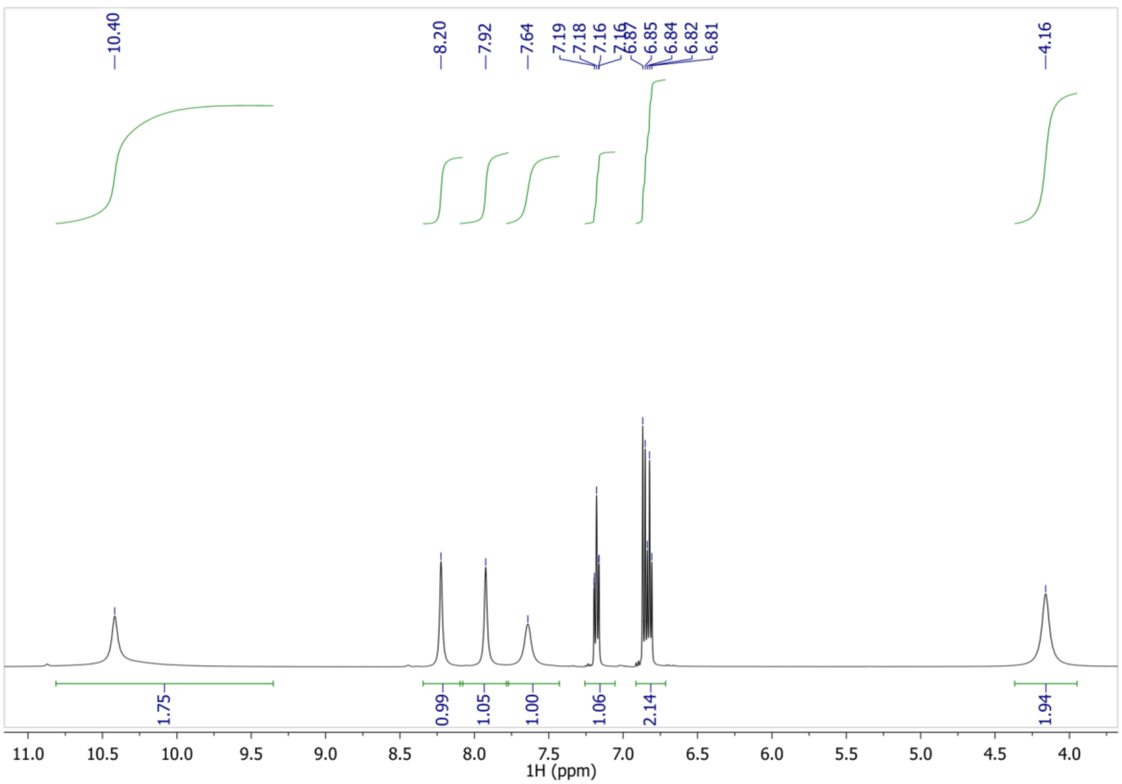

Figure S3. ^{1}H NMR spectrum of **2** in DMSO-d_6.

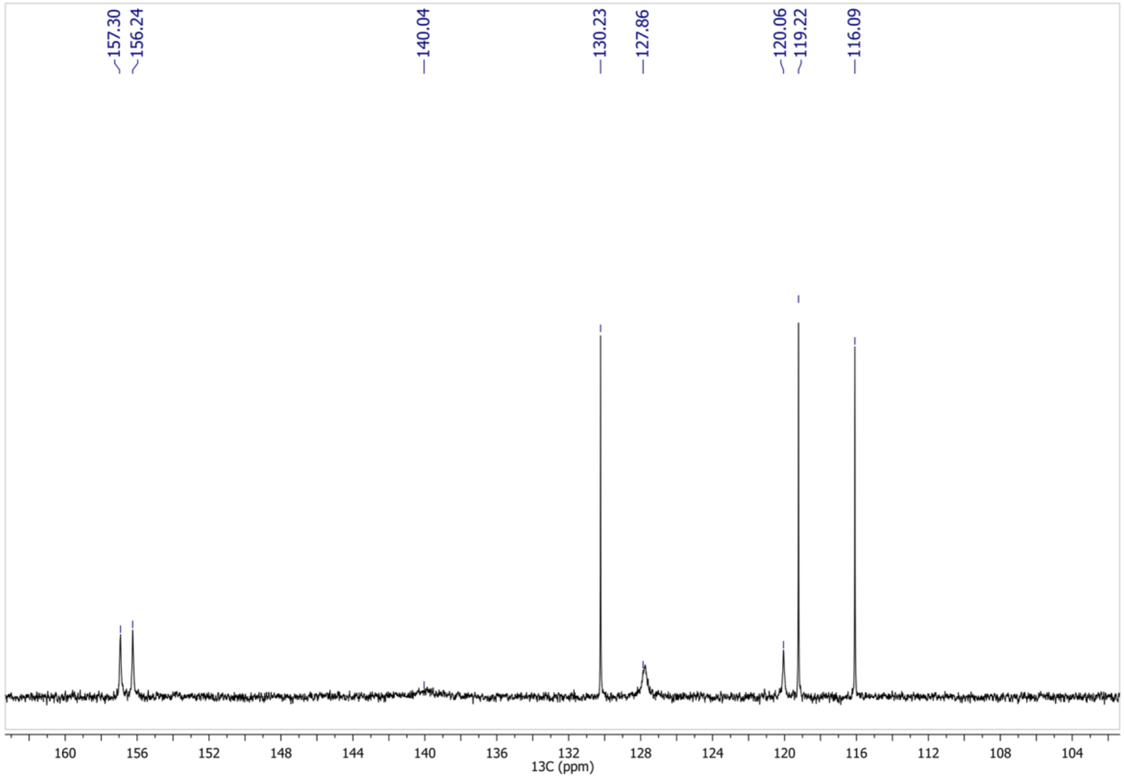

Figure S4. ^{13}C NMR spectrum of **2** in DMSO-d_6.

2-pyridinecarboxaldehyde carbohydrazone (**3**). White solid was recrystallized from acetonitrile. Yield: 67%. M.p. 173-174 °C. Elemental analysis calcd. for $C_7H_9N_{20}O$ (Mw = 179.18 g mol^{-1}): C, 46.92; H, 5.06; N, 39.09%, Found: C, 46.88; H, 5.01; N, 39.11%. IR (KBr, cm^{-1}): 3313s (NH_2), 3208s (NH), 1678vs (C=O), 1635m (C=N).^{1}H NMR (500 MHz, DMSO-d_6, δ (ppm): 4.11 (s, 2H, H2–N5); 7.31 (ddd, 1H, H–C5, $^3J_{5,4}$ = 7.5 Hz, $^3J_{5,6}$ = 4.9 Hz); 7.78 (td, 1H, H–C4, $^3J_{4,3}$ = 7.9 Hz, $^3J_{4,5}$ =7.5 Hz, $^4J_{4,6}$ = 1.5 Hz); 7.89 (s, 1H, H–C7); 8.284-8.105 (br.m.ovlp., 2H, H–C3, H-N4, $^3J_{3,4}$ = 7.9 Hz); 8.51 (ddd, 1H, H–C6, $^3J_{6,5}$ = 4.9 Hz, $^4J_{6,4}$ = 1,5 Hz); 10.64 (s, 1H, H–N3). ^{13}C NMR (126 MHz, DMSO-d_6, δ (ppm): 119.85 (C3); 123.69 (C5); 136.47 (C4); 140.59 (C7); 149.09 (C6); 153.77 (C2); 156.85 (C8). ^{15}N NMR (derived from 2D HMBC, δ / ppm): 51.10 (N_5), 99.70 (N_4), 153.60 (N_3), 312.20 (N_1), 326.00 (N_2) (Božić et al., 2017).

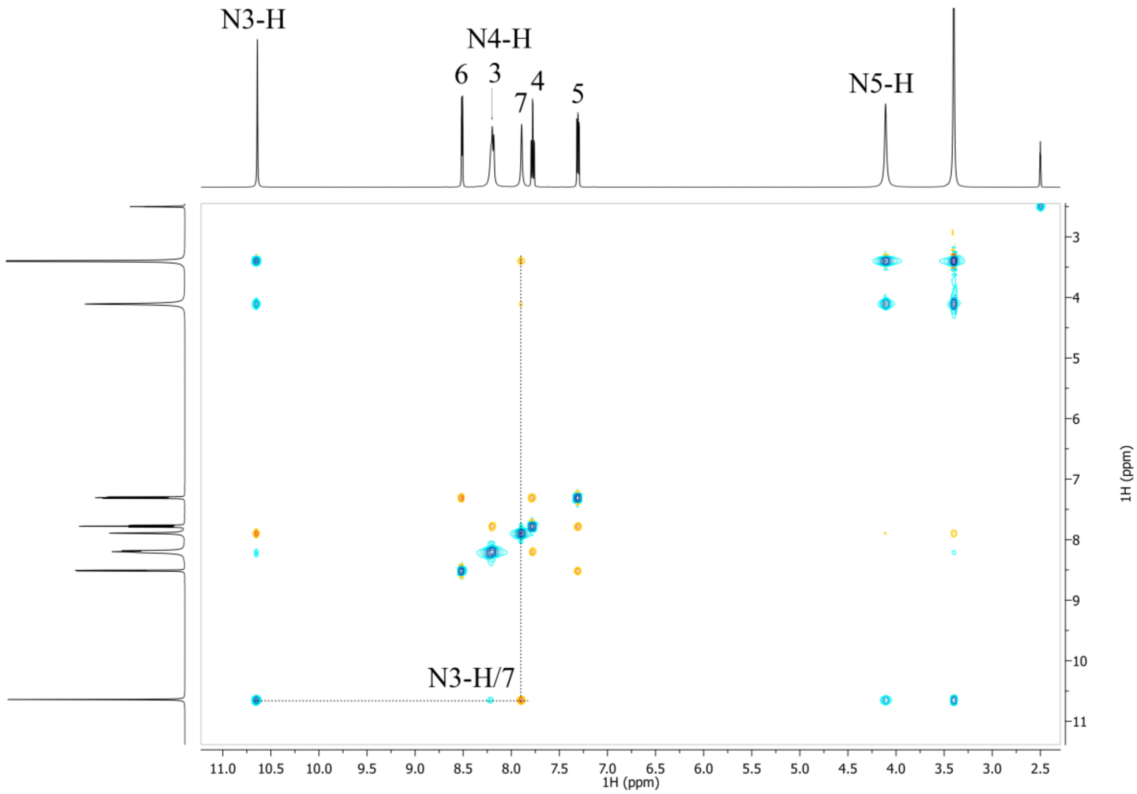

Figure S5. NOESY spectrum of compound **3** in DMSO-d_6.

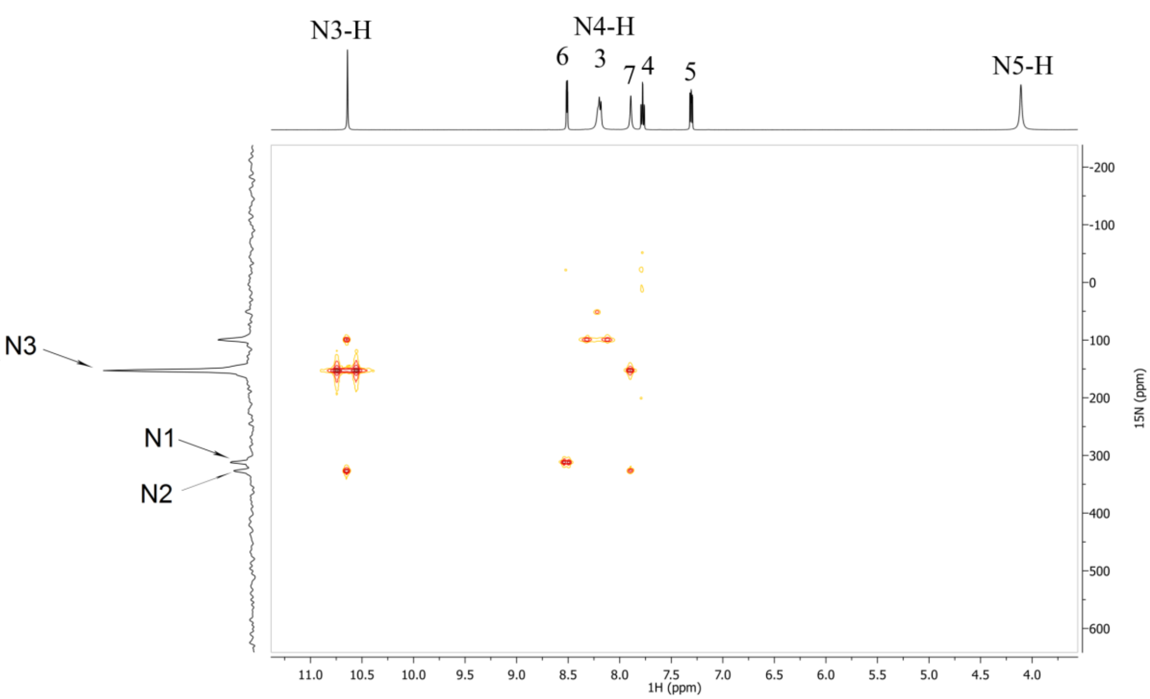

Figure S6. ^{1}H- ^{15}N HMBC spectrum of **3** in DMSO-d_6.

3-pyridinecarboxaldehyde carbohydrazone (**4**)

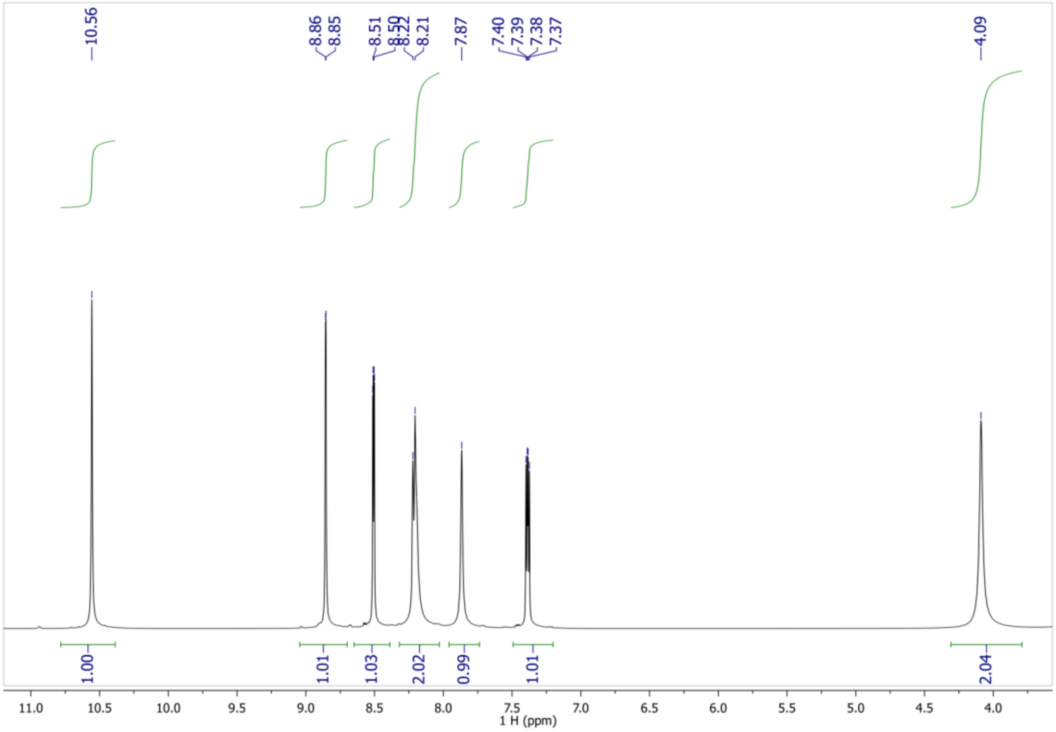

Figure S7. ^{1}H NMR spectrum of **4** in DMSO-d_6.

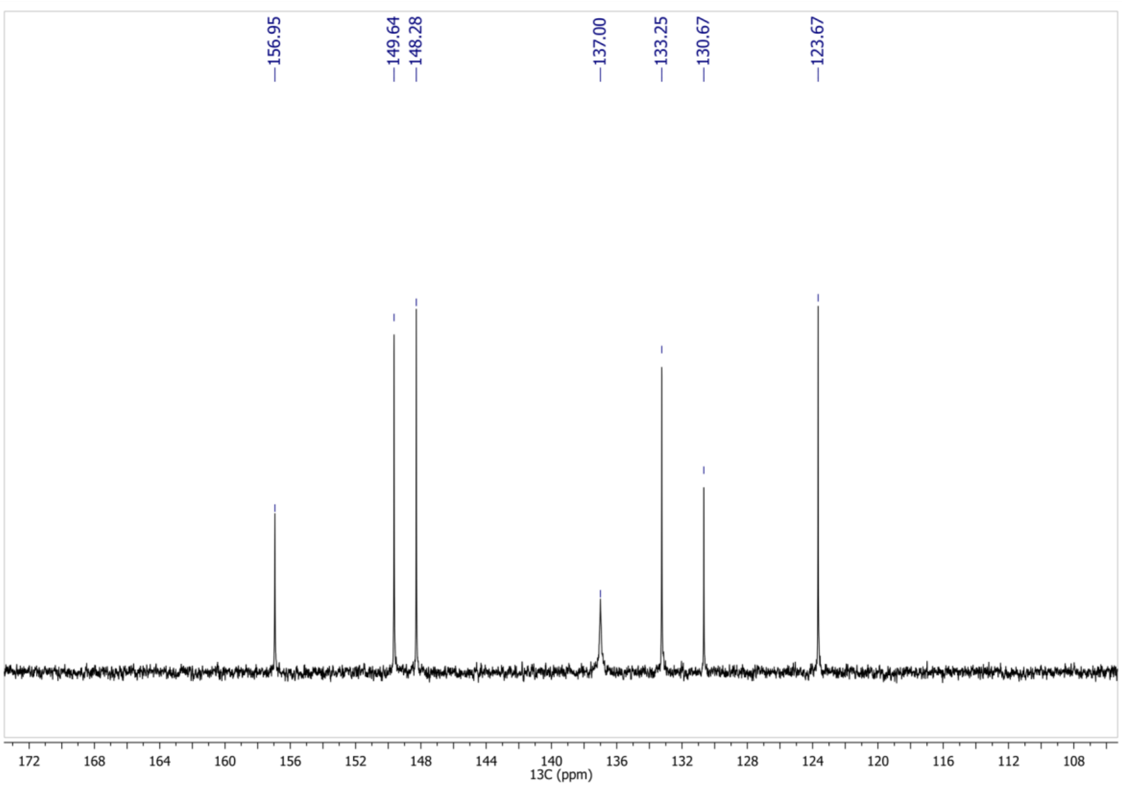

Figure S8. ^{13}C NMR spectrum of **4** in DMSO-d_6.

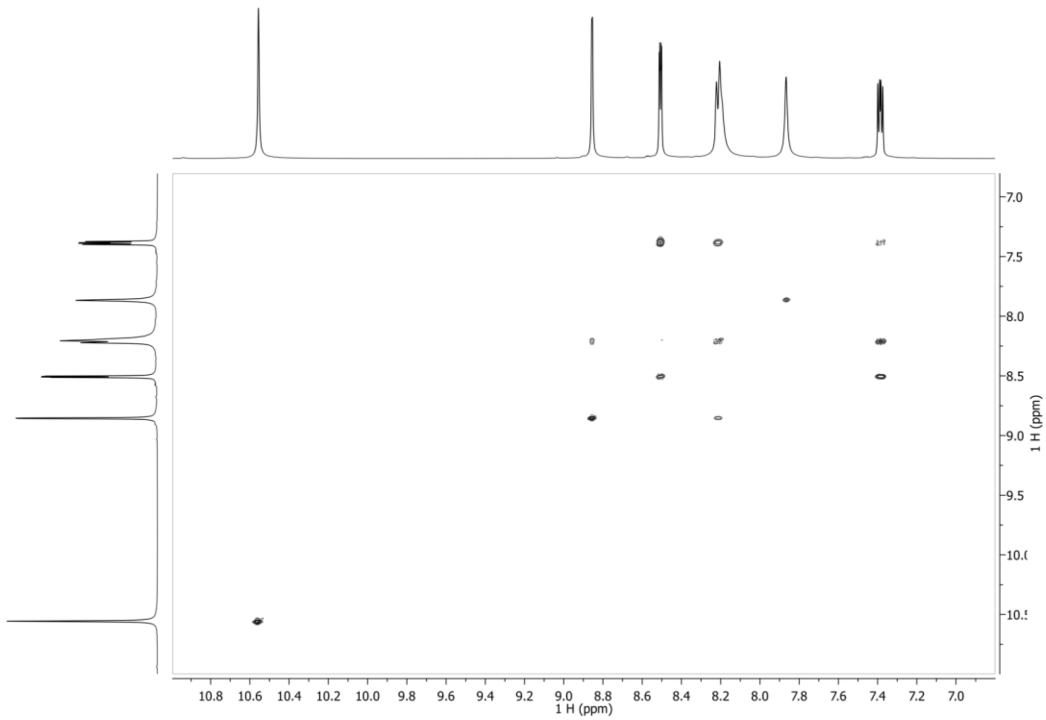

Figure S9. COSY spectrum of **4** in DMSO-d_6

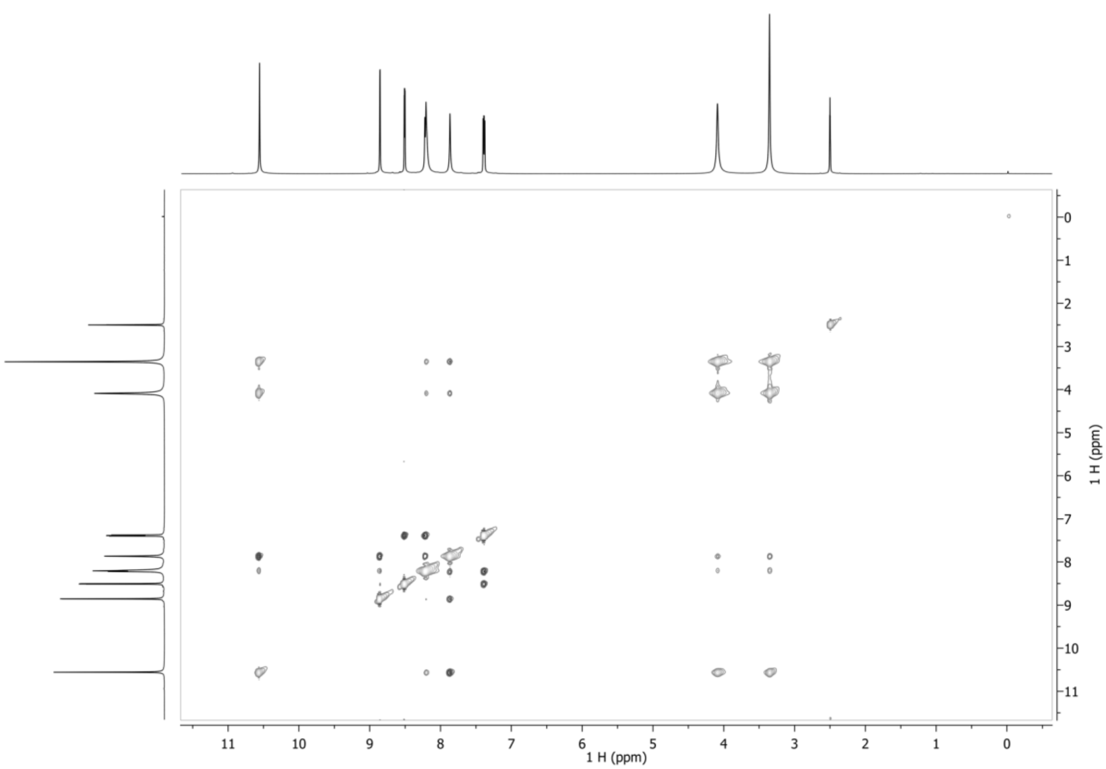

Figure S10. NOESY spectrum of **4** in DMSO-d_6

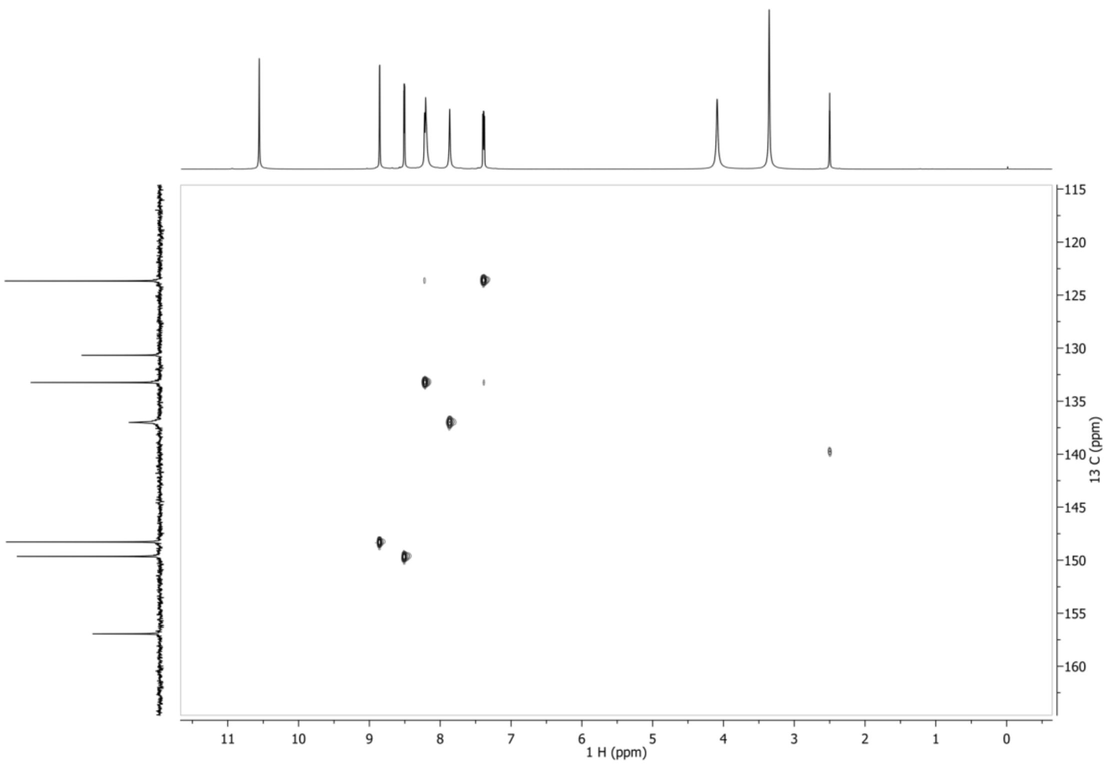

Figure S11. ^{1}H-^{13}C HSQC spectrum of **4** in DMSO-d_6

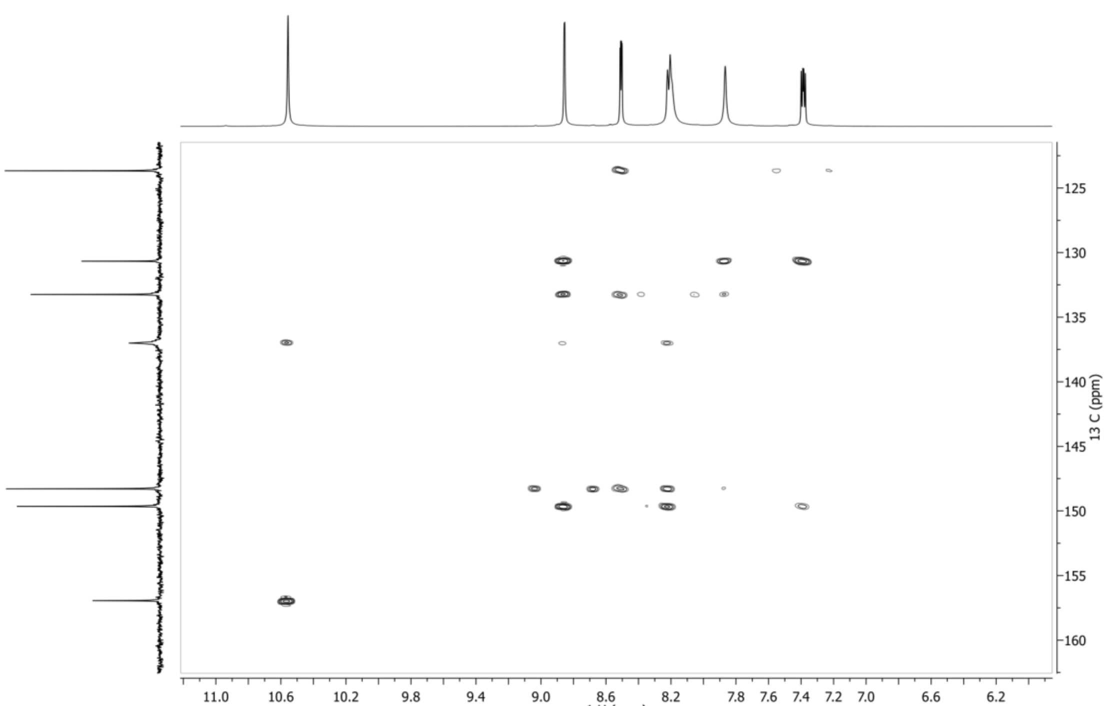

Figure S12. ^{1}H-^{13}C HMBC spectrum of **4** in DMSO-d_6

4-pyridinecarboxaldehyde carbohydrazone (**5**). Yield: 57%. White crystals suitable for single crystal XRD were obtained after recrystallization from absolute ethanol. M.p. 189-190 ^{o}C (lit.M.p. 207-209 ^{o}C). Elemental analysis calcd. for $C_7H_9N_5O$ (*Mw* = 179.18 g mol^{-1}): C, 46.92; H, 5.06; N, 39.09%, Found: C, 46.88; H, 5.04; N, 39.02%. IR (KBr, cm^{-1}): 3314s (NH_2), 3206s (NH), 1683vs (C=O), 1636m (C=N). ^{1}H NMR (DMSO-d_6, δ (ppm): 4,12 (s, 2H, H–N5); 7,71 (d, 2H, H–C3 = H–C5, $^3J_{3,2}$ =$^3J_{5,6}$ =5.5 Hz); 7,86 (s, 1H, H–C7); 8,27 (s, 1H, H–N4); 8,55 (d, 2H, H–C2 = H–C6, $^3J_{2,3}$ =$^3J_{6,5}$ =5.5 Hz); 10,76 (s, 1H, H–N3). ^{13}C NMR (DMSO-d_6, δ (ppm): 120,71 (C3,C5); 137,31 (C7); 141,97 (C4); 149,76 (C2,C6); 156,67 (C8).

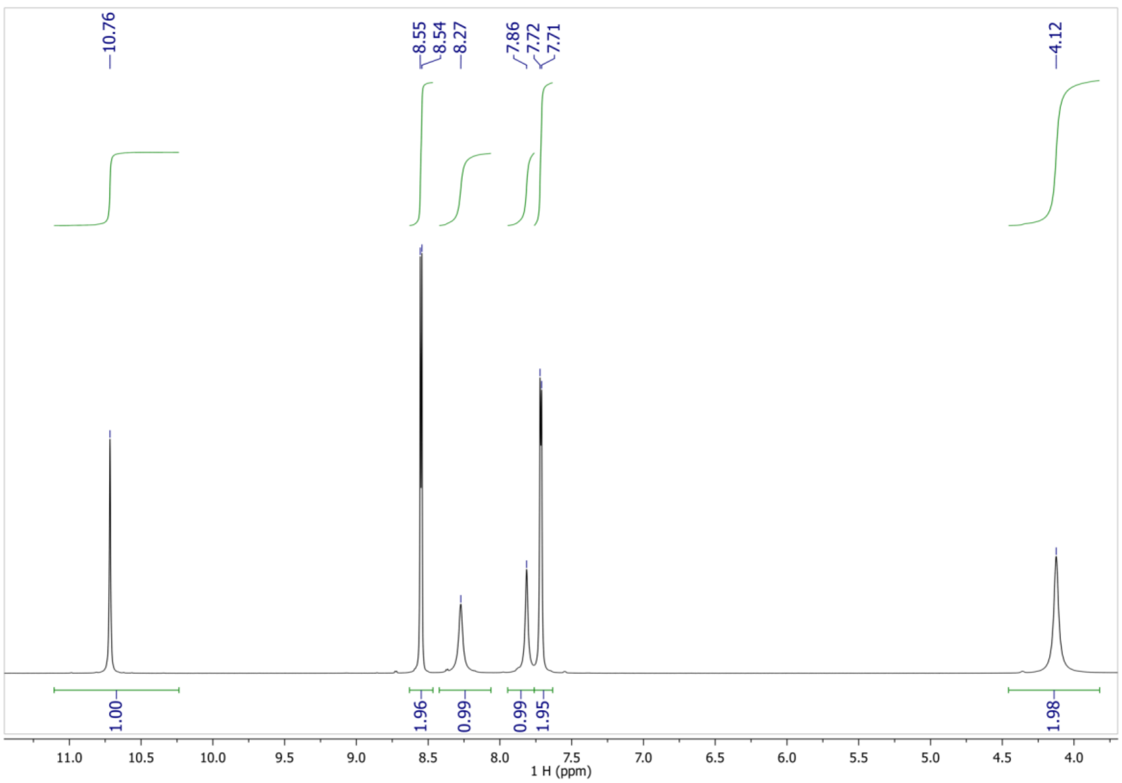

Figure S13. ^{1}H NMR spectrum of **5** in DMSO-d_6.

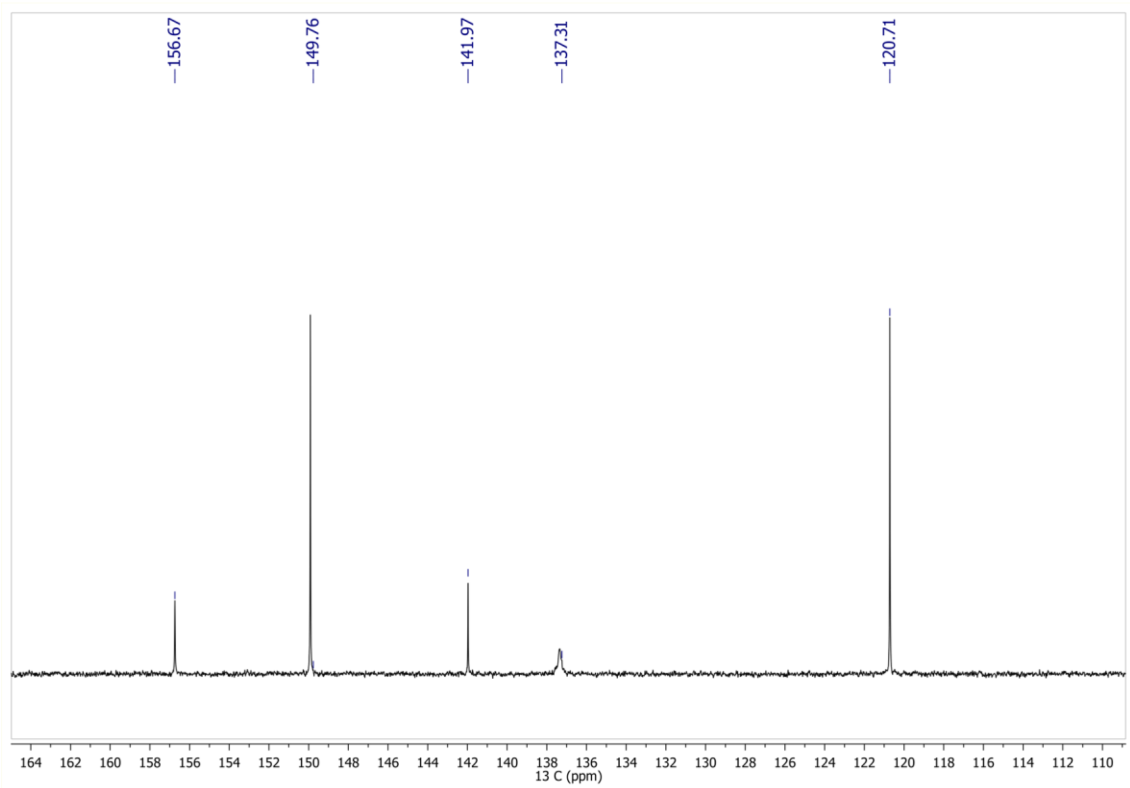

Figure S14. ^{13}C NMR spectrum of **5** in DMSO-d_6.

Methyl phenyl ketone carbohydrazone (**6**). White solid was recrystallized from absolute ethanol. Yield: 68%. M.p. 203-205°C (lit. M.p. 210-212). Elemental analysis calcd. for $C_9H_{12}N_4O$ (Mw = 192.10 g mol^{-1}): C, 56.24; H, 6.29; N, 29.18%; Found: C, 56.16; H, 6.48; N, 29.01 %. IR (KBr, cm^{-1}) ν_{max}: 3275m (NH_2), 3060s (NH), 1674vs (C=O), 1604m (C=N). ^{1}H NMR (500 MHz, DMSO-d_6,) δ (ppm): 2.26 (s, 3H, H-C8); 4.20 (s, 2H, H2–N4); 7.60-7.90 (m, 5H, H–C2-C6); 8.10 (s, 1H, H–N3); 9.50 (s. 1H, H-N2). ^{13}C NMR (126 MHz, DMSO-d_6) δ (ppm): 13.1 (C8); 126.13 (C3=C5); 129.06 (C2=C6); 131.86 (C1); 138.30 (C1); 145.41 (C7); 157.69 (C8).

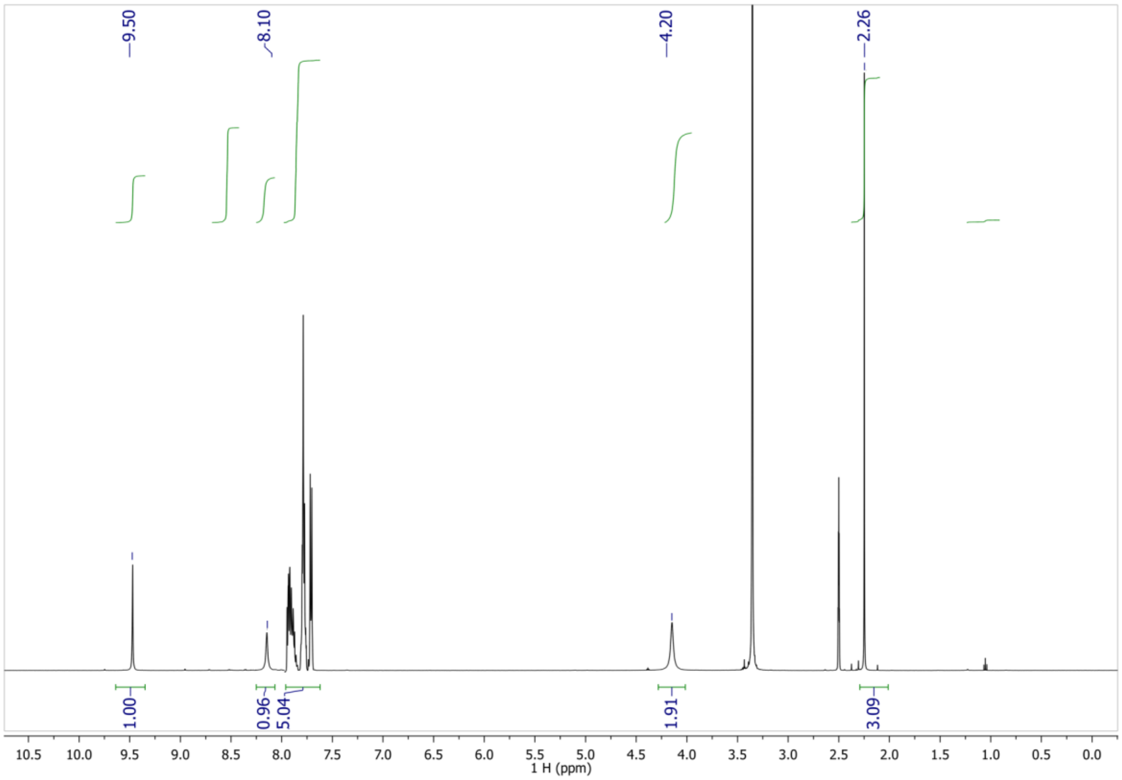

Figure S15. ^{1}H NMR spectrum of **6** in DMSO-d_6.

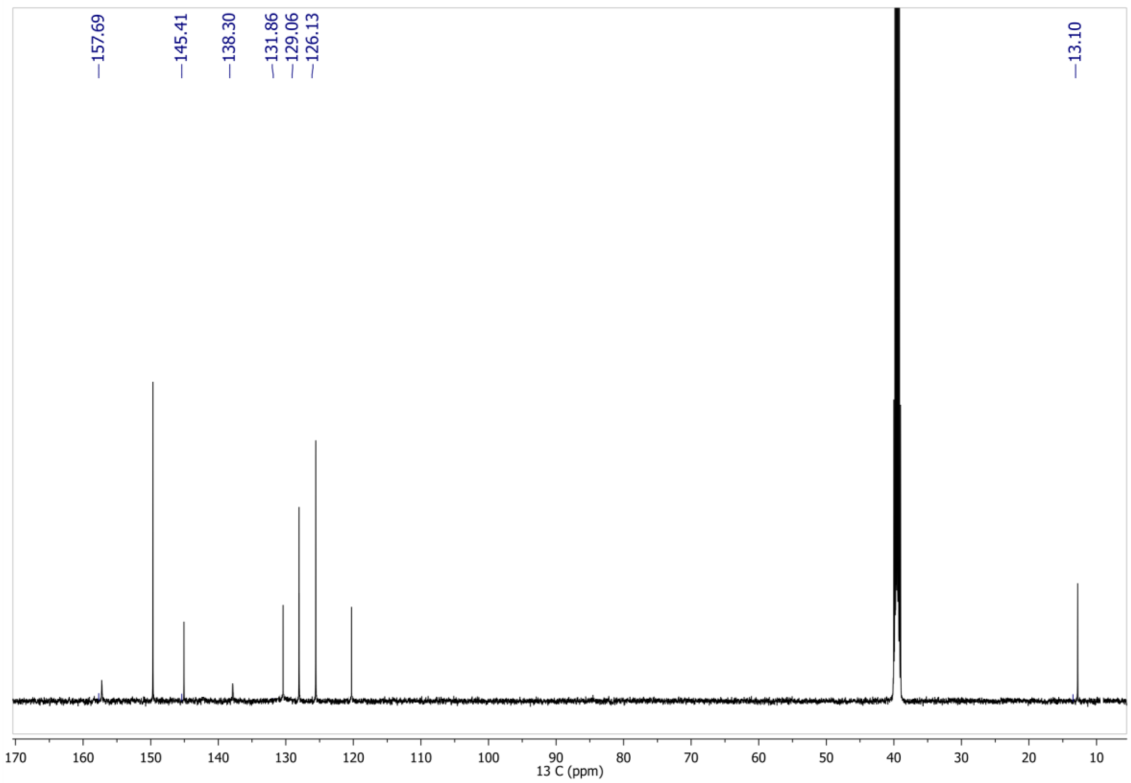

Figure S16. ^{13}C NMR spectrum of **6** in DMSO-d_6.

Methyl 2-pyridyl ketone carbohydrazone (**7**). White solid was recrystallized from absolute methanol. Yield: 72,0 %. M.p. 202-203 ^{o}C (lit M.p. 202-203 ^{o}C). Elemental analysis calcd. for $C_8H_{11}N_5O$ (Mw = 193.21 g mol^{-1}): C, 47.73; H, 5.74; N, 36.25%, Found: C, 47.61; H, 5.82; N, 36.18%. IR (KBr, cm^{-1}) v_{max}: 3308m (NH_2), 3197m (NH), 3037w (CH_{aryl}), 1674vs (C=O), 1631m (C=N). ^{1}H NMR (300 MHz, DMSO-d_6, δ (ppm): 2.26 (s, 3H, H-C8); 4.14 (s, 2H, H–N5); 7.34 (dd, 1H, H–C5); 7.76 (td, 1H, H–C4); 8.18 (s, 1H, H-N4); 8.38 (d, 1H, H–C6); 8.52 (d, 1H, H–C3); 9.76 (s, 1H, H–N3). ^{13}C NMR (126 MHz, DMSO-d_6, δ (ppm): 11.60 (C8); 120.51 (C3); 123.69 (C5); 136.26 (C4); 145.19 (C7); 148.35 (C6); 155.07 (C2); 157.41 (C9).

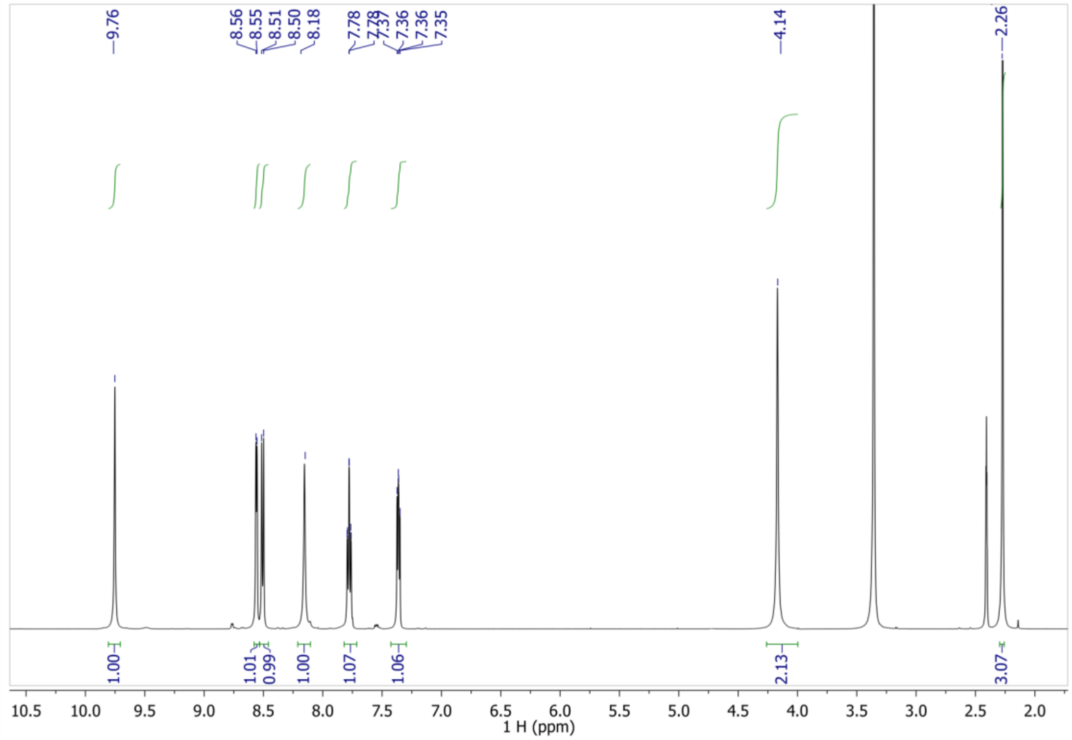

Figure S17. ^{13}C NMR spectrum of **7** in DMSO-d_6.

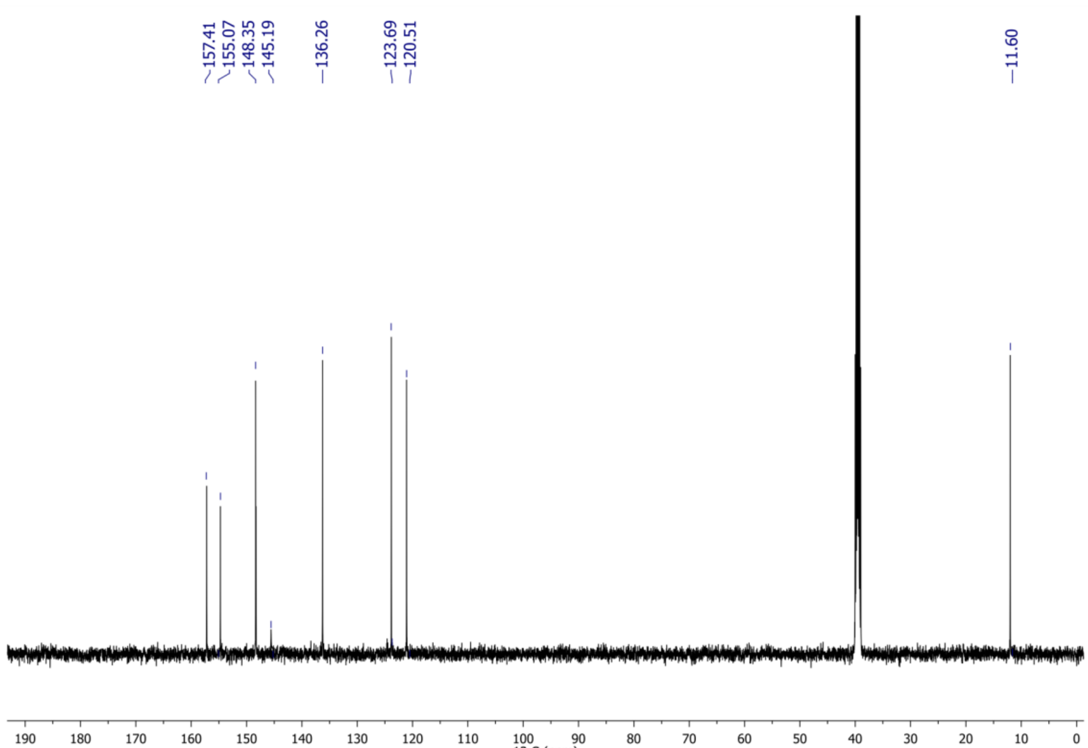

Figure S18. ^{13}C NMR spectrum of **7** in DMSO-d_6.

*Methyl 3-pyridyl ketone carbohydrazone (**8**)*

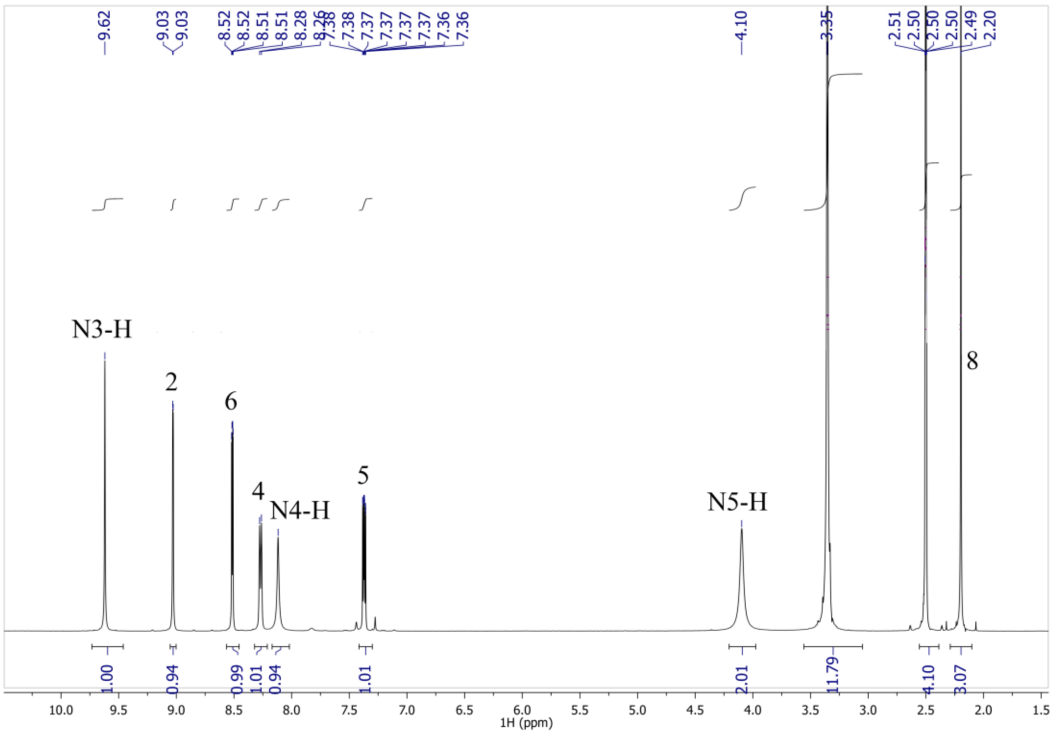

Figure S19. ^{1}H NMR spectrum of **8** in DMSO-d_6.

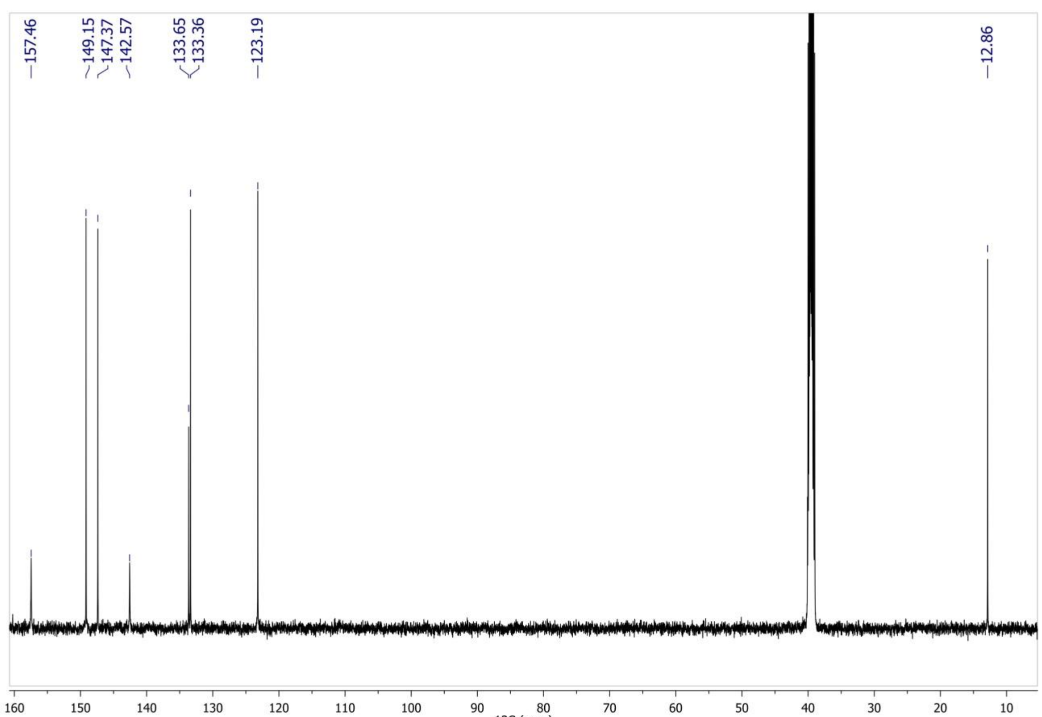

Figure S20. ^{13}C NMR spectrum of **8** in DMSO-d_6.

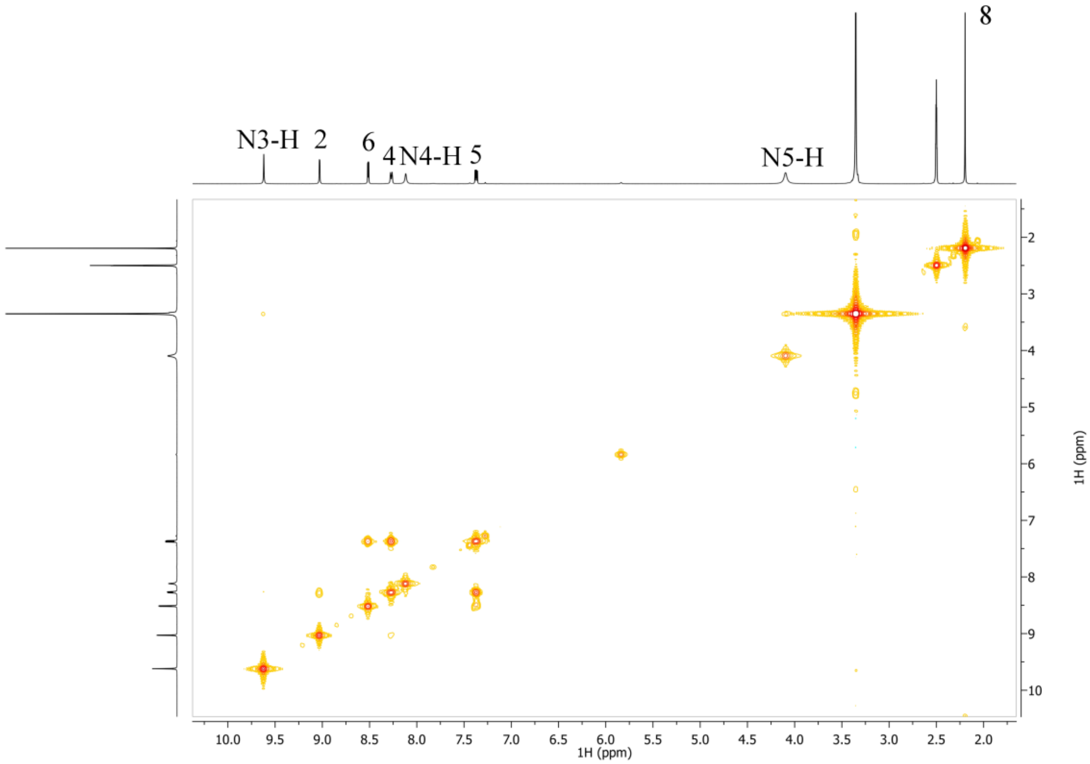

Figure S21. COSY spectrum of **8** in DMSO-d_6

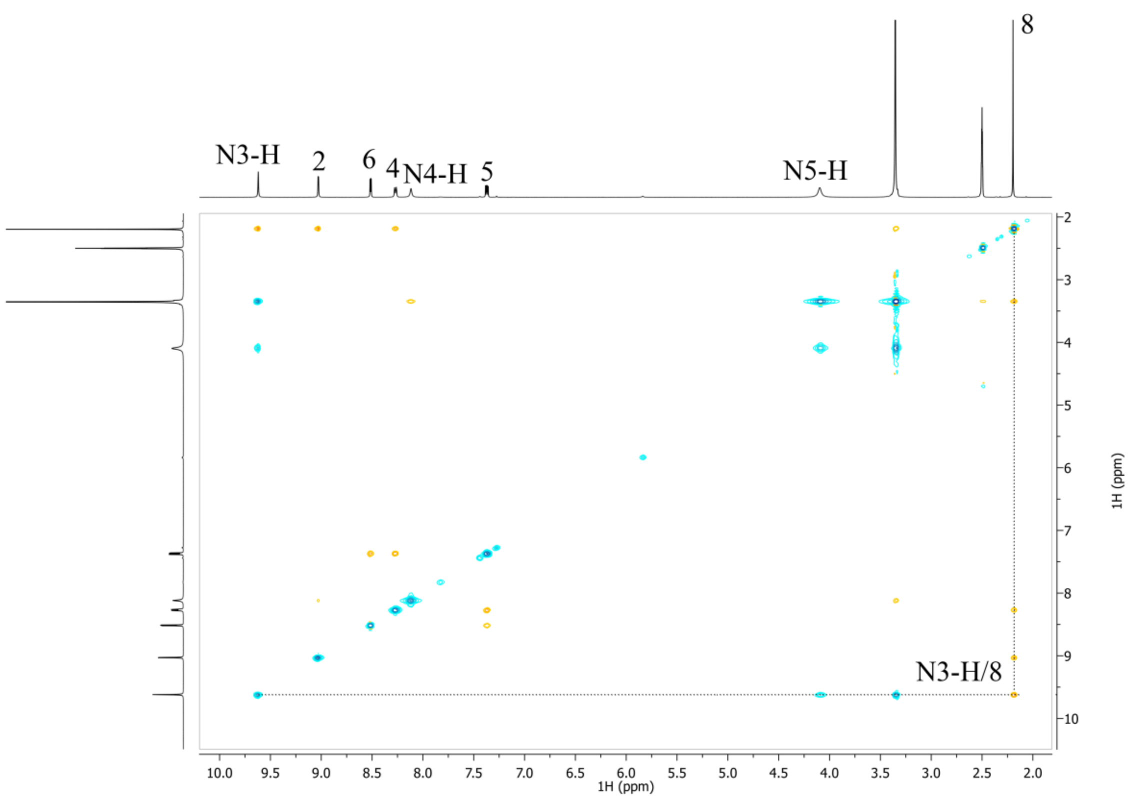

Figure S22. NOESY spectrum of **8** in DMSO-d_6.

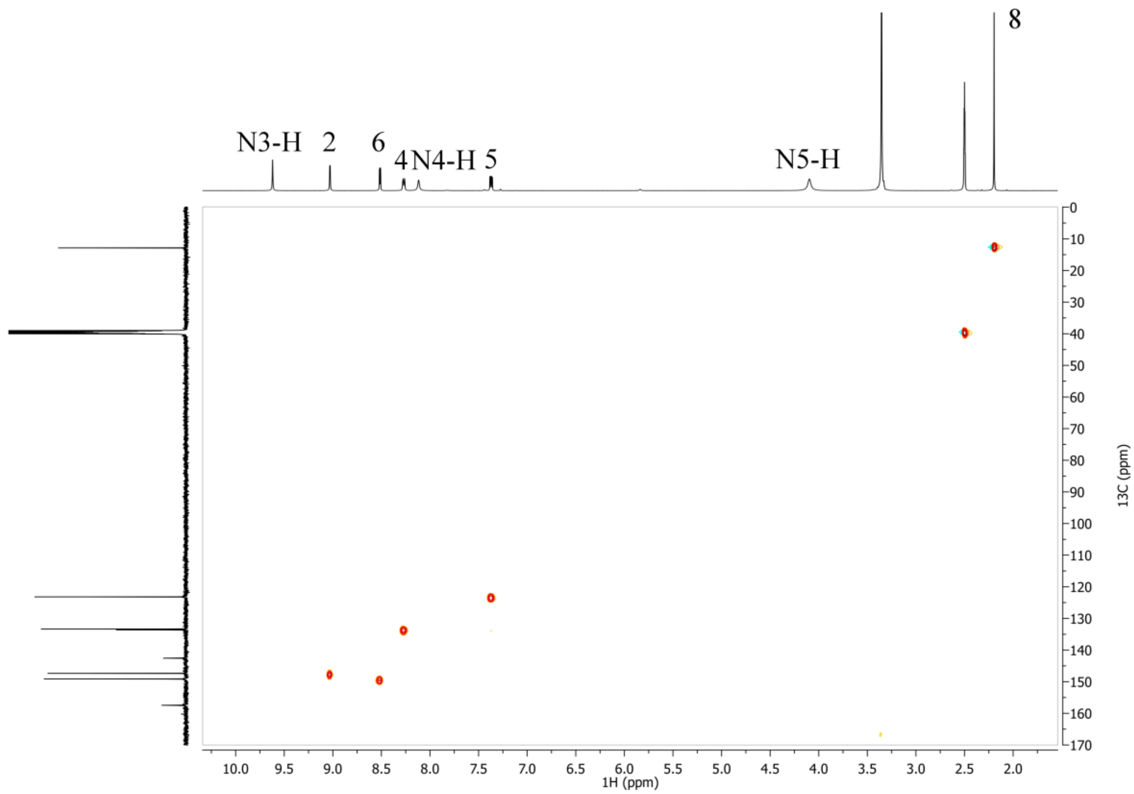

Figure S23. ^{1}H - ^{13}C HSQC spectrum of **8** in DMSO-d_6.

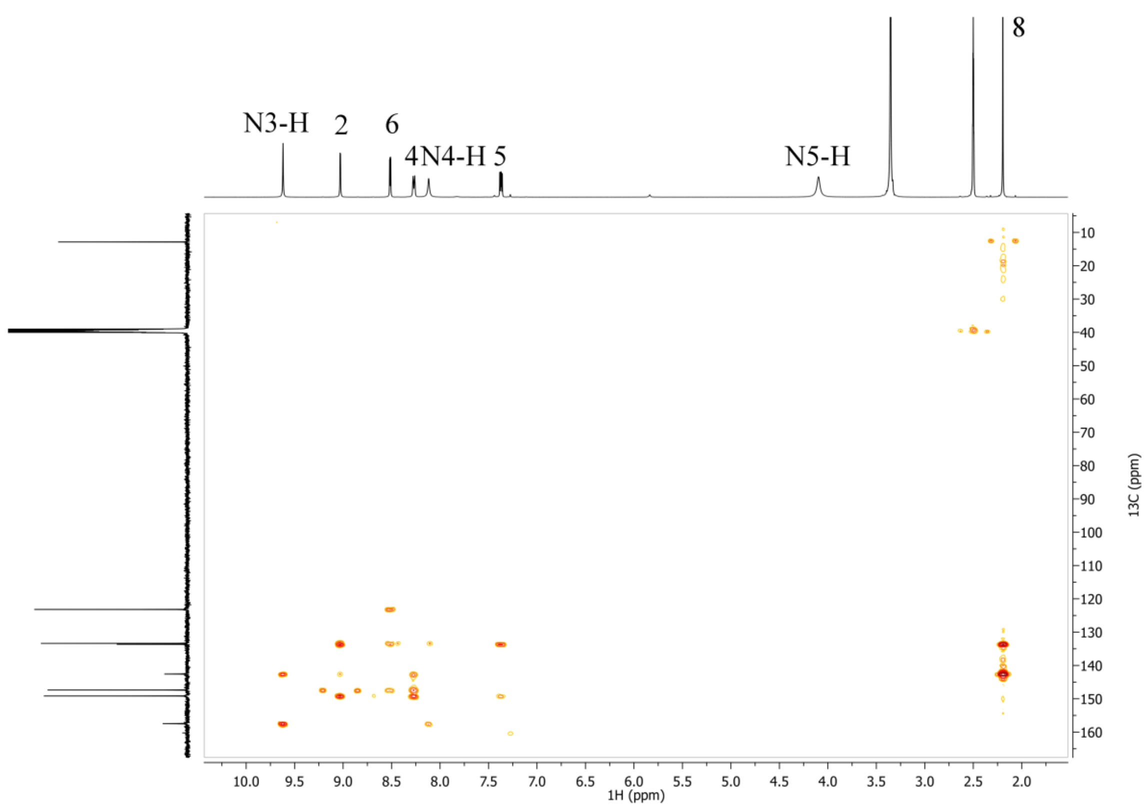

Figure S24. ^{1}H - ^{13}C HMBC spectrum of **8** in DMSO-d_6.

*Methyl 4-pyridyl ketone carbohydrazone (**9**).* Yield: 84,0%. White crystals was obtained after recrystallization compound from absolute ethanol. M.p. 208-209 °C (lit. M.p. – no data). Elemental analysis calcd. for $C_8H_{11}N_5O$ (*Mw* = 193.21 g mol^{-1}): C, 47.73; H, 5.74; N, 36.25%, Found: C, 47.52; H, 5.74; N, 36.29%. IR (KBr, cm^{-1}) ν_{max}: 3314m (NH_2), 3206m (NH), 3037w (CH_{aryl}), 1681vs (C=O), 1631m (C=N). ^{1}H NMR (500 MHz, DMSO-d_6, δ (ppm): 2.17 (s, 3H, H-C8); 4.12 (s, 2H, H–N5); 7.84 (d, 2H, H–C3, H–C5, $^3J_{3,2}$ =$^3J_{5,6}$ = 6.0 Hz); 8.20 (s, 1H, H–N4); 8.54 (d, 2H, H–C2 = H–C6, $^3J_{2,3}$ =$^3J_{6,5}$ = 6.0 Hz); 9.76 (s, 1H, H–N3). ^{13}C NMR (126 MHz, DMSO-d_6, δ (ppm): 12.42 (C8); 120.27 (C3,C5); 142.22 (C7); 145.07 (C4); 149.75 (C2,C6); 157.33 (C9).

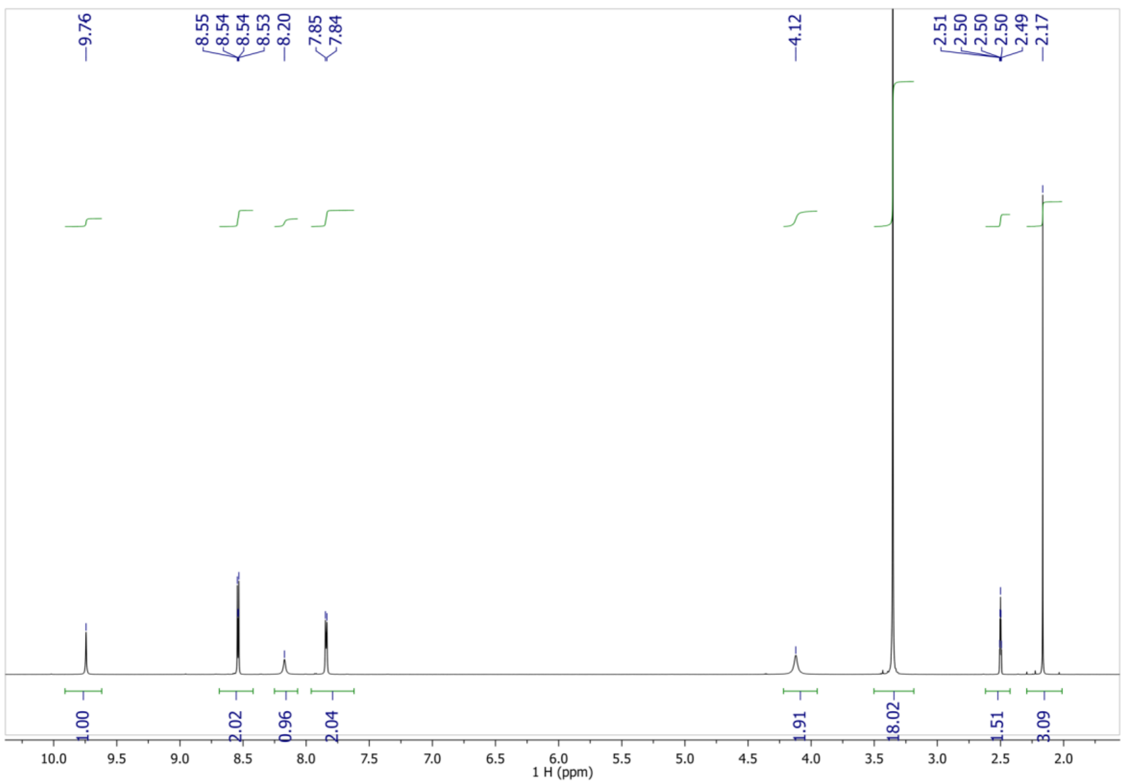

Figure S25. ^{1}H NMR spectrum of **9** in DMSO-d_6.

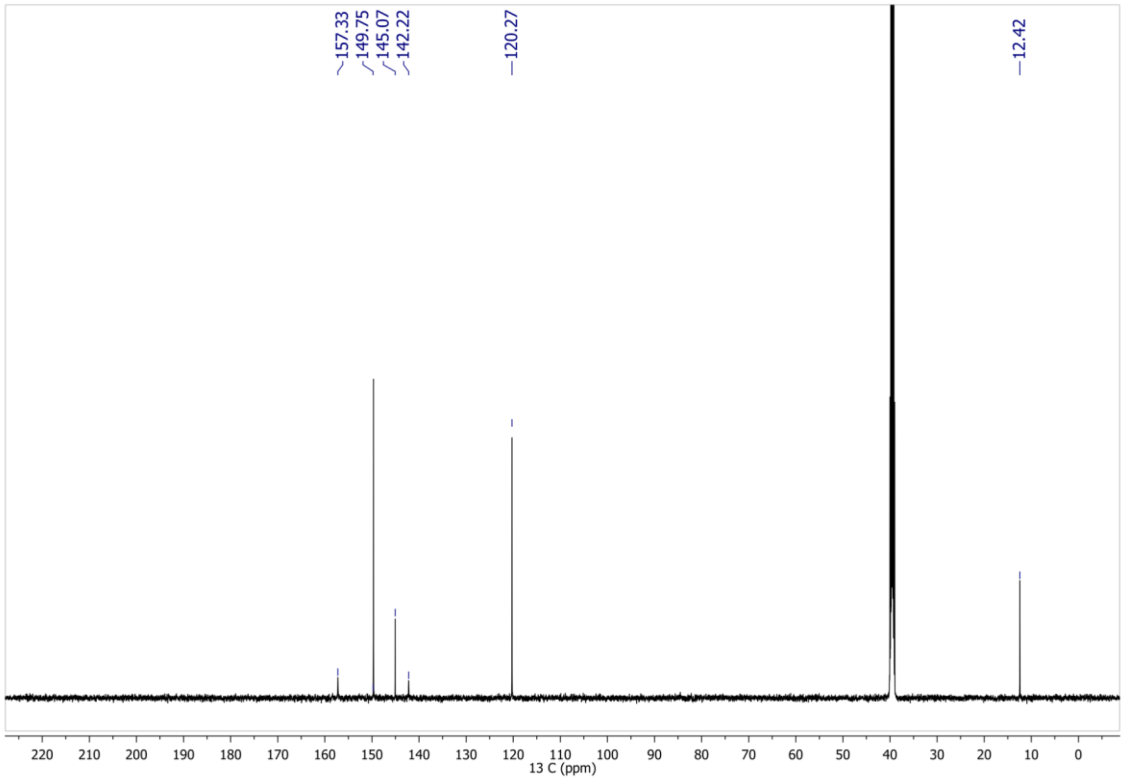

Figure S26. ^{13}C NMR spectrum of **9** in DMSO-d_6.

8-Quinolinealdehyde carbohydrazone (**10**). Yelow solid was recrystallized from absolute methanol. Yield: 64%. M.p. 185 °C. Elemental analysis calcd. for $C_{11}H_{11}N_5O$ (*Mw* = 229.24 g mol^{-1}): C, 57.63; H, 4.84; N, 30.55%; Found: C, 57.71; H, 4.78; N, 30.62%. IR (KBr, cm^{-1}) ν_{max}: 3316s (NH_2), 3200s (NH), 1681vs (C=O), 1621m (C=N). ^1H NMR (500.26 MHz, DMSO-d_6,) δ (ppm): 4.12 (s, 2H, H–N5), 7.57 (dd, 1H, H–C3, $^3J_{3,4}$ = 8.3 Hz, $^3J_{3,2}$ = 4.1 Hz), 7.63 (t, 1H, H–C6, $^3J_{6,5}$ = $^3J_{6,7}$ = 7.4 Hz), 7.98 (dd, 1H, H–C5, $^3J_{5,6}$ =7.8 Hz, $^4J_{5,7}$ =1 Hz), 8.16 (s, 1H, H–N4), 8.39 (dd, 1H, H–C4, $^3J_{4,3}$ = 8.3 Hz, $^4J_{4,2}$ =2.0 Hz), 8.58 (d, 1H, H–C7, $^3J_{7,6}$ = 7.4 Hz), 8.94 (dd, 1H, H–C2, $^3J_{2,3}$ = 4.1 Hz, $^3J_{2,4}$ = 2.0 Hz), 9.14 (s, 1H, H–C9), 10.65 (s, 1H, H–N3). ^{13}C NMR (126 MHz, DMSO-d_6, δ (ppm): 121.67 (C3), 125.61 (C7), 126.45 (C6), 127.94 (C4a), 128.90 (C5), 131.59 (C8), 136.55 (C4), 136.89 (C9), 145.01 (C8a), 150.08 (C2), 157.21 (C10). (Božić et al., 2016).

2-Quinolinealdehyde carbohydrazone (**11**). Yelow solid was recrystallized from absolute ethanol. Yield: 56%. M.p. 183 °C. Elemental analysis calcd. for $C_{11}H_{11}N_5O$ (*Mw* = 229.24 g mol^{-1}): C, 57.63; H, 4.84; N, 30.55%, Found: C, 57.58; H, 4.62; N, 30.69%. IR (KBr, cm^{-1}) ν_{max}: 3297s (NH_2), 3188s (NH), 1679vs (C=O), 1638m (C=N).^{1}H NMR (500.26 MHz, DMSO-d_6,) δ (ppm): 4.15 (s, 2H, H–N5), 7.58 (ddd, 1H, H–C6, $^{3}J_{6,7}$ = 8,2 Hz), 7.74 (ddd, 1H, H–C7, $^{3}J_{7,6}$ = 8.2 Hz), 7.93-7.99 (br.m.ovlp. 2H, H–C5, H–C8), 8.03 (s, 1H, H–C9), 8.27 (d, 1H, H–C4, $^{3}J_{4,3}$ = 8.4 Hz), 8.34-8.46 (br.m.ovlp. 2H, H–C3, H–N4, $^{3}J_{3,4}$ = 8,4 Hz), 10.84 (s, 1H, H–N3). ^{13}C NMR (126 MHz, DMSO-d_6, δ (ppm): 118.03 (C3), 126.84 (C6), 127.66 (4a), 127.92 (C5), 128.69 (C8), 129.82 (C7), 136.19 (C4), 140.64 (C9), 147.26 (C8a), 154.34 (C2), 156.76 (C10). (Božić et al., 2016).

8-Hydroxy-2-quinolinealdehyde carbohydrazone (**12**). Yelow solid was recrystallized from absolute methanol. Yield: 72%. M.p. 214-215 °C. Elemental analysis calcd. for $C_{11}H_{11}N_5O_2$ (*Mw* = 245.24 g mol^{-1}): C, 53.83; H, 4.525; N, 28.56%; Found: C, 53.66; H, 4.68; N, 28.74%. IR (KBr, cm^{-1}) ν_{max}: 3371s (OH), 3335s (NH_2), 3198s (NH), 1696vs (C=O), 1600m (C=N).^{1}H NMR (500.26 MHz, DMSO-d_6,) δ (ppm): 4.14 (s, 2H, H–N5), 7.08 (dd, 1H, H–C7, $^{4}J_{7,5}$ = 1.4 Hz), 7.36 (dd, 1H, H–C5, $^{4}J_{5,7}$ = 1.4 Hz), 7.41 (m, 1H, H–C6), 8.09 (s, 1H, H–C9), 8.24 (d, 1H, H–C4, $^{3}J_{4,3}$ = 8.55 Hz), 8.30-8.50 (br.m.ovlp., 2H, H–C3, H–N4, $^{3}J_{3,4}$ = 8.55 Hz), 9.71 (s, 1H, OH), 10.88 (s, 1H, H–N3). ^{13}C NMR (126 MHz, DMSO-d_6, δ (ppm): 111.59 (C7), 117.74 (C5), 118.35 (C3), 127.73 (C6), 128.52 (C4a), 136.06 (C4), 137.93 (C8a), 140.50 (C9), 152.25 (C2), 153.24 (C8), 156.83 (C10). (Božić et al., 2016).

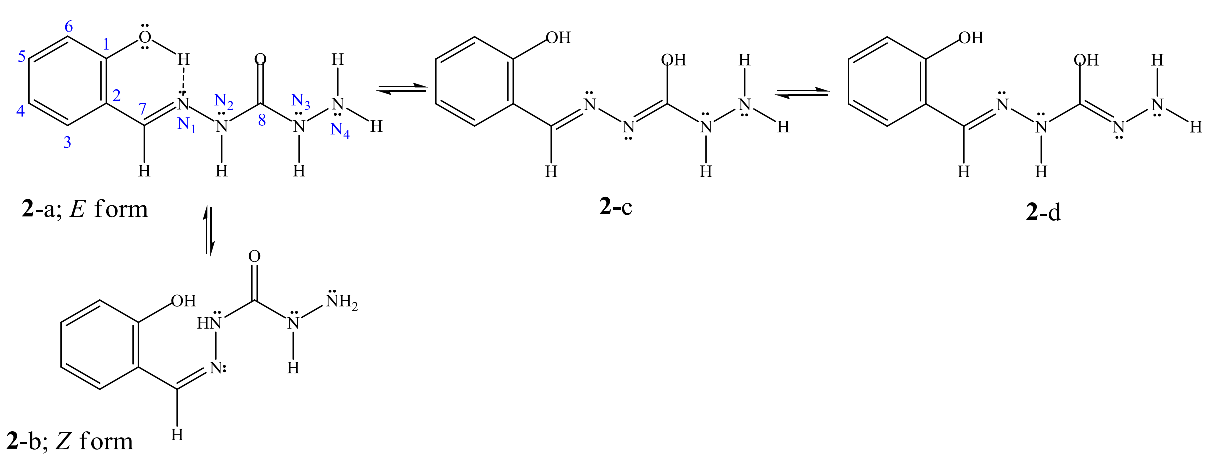

Figure S27. Equilibrium of tautomeric forms and geometrical isomers of **2** with numeration of the atom of interest.

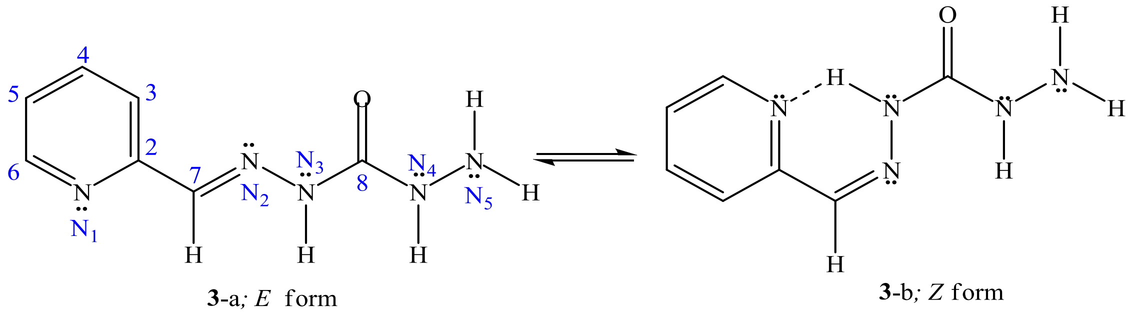

Figure S28. *E*-isomer of compound **3** with numeration of atoms of interest.

*Crystal structures of compounds **5** and **9***

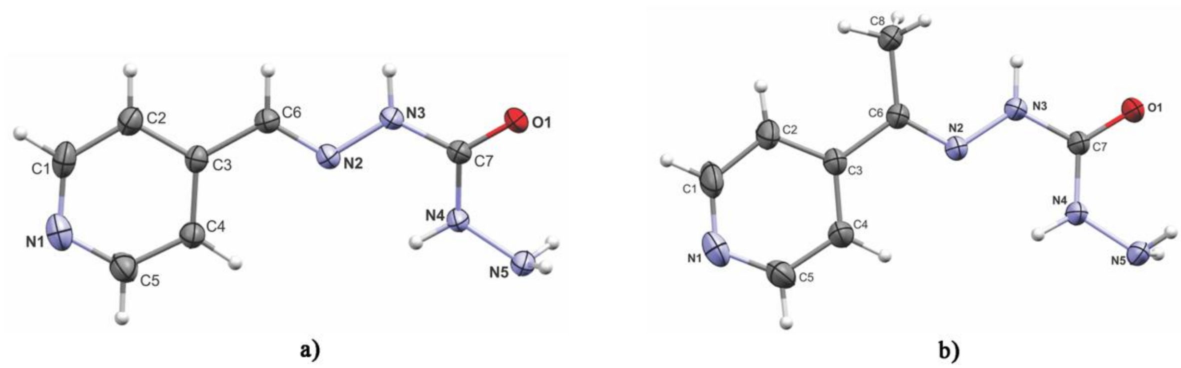

Figure S29. ORTEP (Farrugia, 1997) drawings of the molecular structures of compounds 5 (a) and 9 (b) with labeling of non-H atoms. Displacement ellipsoids are shown at the 50% probability level and H atoms are drawn as spheres of arbitrary radii.

Table S5. Selected bond lengths (Å) and angles (°).

5		9	
Bond		***Bond***	
O1—C7	1.2308 (17)	O1—C7	1.2285 (18)
N2—C6	1.274 (2)	N2—C6	1.284 (2)
N2—N3	1.3646 (17)	N2—N3	1.3678 (18)
N3—C7	1.367 (2)	N3—C7	1.3702 (19)
N4—C7	1.3425 (19)	N4—C7	1.345 (2)
N4—N5	1.4098 (19)	N4—N5	1.406 (2)
C6—C3	1.458 (2)	C6—C3	1.483 (2)
		C6—C8	1.497 (2)
C3—C2	1.383 (2)	C3—C2	1.383 (2)
C3—C4	1.390 (2)	C3—C4	1.392 (2)
N1—C1	1.323 (2)	N1—C1	1.325 (3)
N1—C5	1.335 (2)	N1—C5	1.330 (3)
C4—C5	1.368 (2)	C4—C5	1.374 (3)
C2—C1	1.378 (2)	C2—C1	1.384 (3)
Angle		***Angle***	
C6—N2—N3	116.87 (13)	C6—N2—N3	118.44 (13)
N2—N3—C7	119.85 (13)	N2—N3—C7	118.72 (13)
C7—N4—N5	121.43 (14)	C7—N4—N5	121.22 (14)
O1—C7—N4	123.89 (15)	O1—C7—N4	123.24 (14)
O1—C7—N3	120.41 (14)	O1—C7—N3	120.75 (14)
N4—C7—N3	115.69 (13)	N4—C7—N3	116.01 (13)
N2—C6—C3	120.41 (14)	N2—C6—C3	115.42 (14)
		N2—C6—C8	124.48 (14)
		C3—C6—C8	120.10 (13)
C2—C3—C4	117.12 (15)	C2—C3—C4	116.84 (16)
C2—C3—C6	120.51 (15)	C2—C3—C6	122.01 (16)
C4—C3—C6	122.31 (14)	C4—C3—C6	121.09 (15)
C1—N1—C5	115.66 (16)	C1—N1—C5	114.98 (17)
C5—C4—C3	118.67 (16)	C5—C4—C3	118.91 (18)
C1—C2—C3	119.35 (17)	C1—C2—C3	119.0 (2)
N1—C5—C4	124.94 (17)	N1—C5—C4	125.2 (2)
N1—C1—C2	124.19 (18)	N1—C1—C2	125.0 (2)
Torsion angle		***Torsion angle***	
C6—N2—N3—C7	-177.00 (15)	C6—N2—N3—C7	177.51 (15)
N5—N4—C7—O1	5.5 (3)	N5—N4—C7—O1	8.3 (3)
N5—N4—C7—N3	-175.30 (16)	N5—N4—C7—N3	-171.47 (17)
N2—N3—C7—O1	-174.15 (15)	N2—N3—C7—O1	177.27 (15)
N2—N3—C7—N4	6.7 (2)	N2—N3—C7—N4	-2.9 (2)
N3—N2—C6—C3	-174.73 (14)	N3—N2—C6—C3	176.53 (14)
		N3—N2—C6—C8	-2.5 (3)
C2—C3—C6—N2	177.24 (16)	N2—C6—C3—C2	-173.38 (17)
		C8—C6—C3—C2	5.7 (3)
C4—C3—C6—N2	0.2 (3)	N2—C6—C3—C4	3.9 (2)
		C8—C6—C3—C4	-177.02 (17)
C2—C3—C4—C5	-1.3 (2)	C2—C3—C4—C5	0.2 (3)
C6—C3—C4—C5	175.76 (17)	C6—C3—C4—C5	-177.19 (18)
C4—C3—C2—C1	2.1 (2)	C4—C3—C2—C1	-1.4 (3)
C6—C3—C2—C1	-175.07 (16)	C6—C3—C2—C1	176.04 (18)
C1—N1—C5—C4	2.8 (3)	C1—N1—C5—C4	-1.6 (4)
C3—C4—C5—N1	-1.2 (3)	C3—C4—C5—N1	1.3 (4)
C5—N1—C1—C2	-1.9 (3)	C5—N1—C1—C2	0.3 (4)
C3—C2—C1—N1	-0.5 (3)	C3—C2—C1—N1	1.1 (4)

Geometry optimization of mCHs

Table S6. Geometrical data for the most stable *E* isomer of monocarbohydrazones obtained by MP2/6-311G(d,p) method.

Compound/parameter	**1**	**2**	**3**	**4**	**5**	**5*** **	**6**	**7**	**8**	**9**	**9*** **	**10**	**11**	**12**
Bond distance (A°)														
H-C7(C9*)	1.096	1.093	1.093	1.094	1.094	0.930						1.091	1.093	1.093
H-N3(N2**)	1.016	1.012	1.014	1.013	1.014	0.884	1.014	1.012	1.013	1.012	0.910	1.014	1.014	1.014
H-N4(N3**)	1.011	1.007	1.007	1.007	1.007	0.871	1.011	1.007	1.015	1.007	0.861	1.007	1.007	1.007
C2-C7(C9*)	1.462	1.459	1.471				1.477	1.491					1.471	1.469
C3-C7				1.466					1.489					
C4-C7					1.468	1.458				1.485	1.483			
C7-C9												1.468		
C7-C8							1.506	1.501	1.516	1.504	1.497			
C7(9*)-N2(N1**)	1.293	1.278	1.274	1.274	1.275	1.274	1.301	1.281	1.300	1.281	1.284	1.276	1.274	1.275
N2(N1**)-N3(N2**)	1.366	1.350	1.347	1.349	1.344	1.365	1.372	1.349	1.350	1.349	1.368	1.351	1.344	1.343
N3(N2**)-C(=O)	1.394	1.384	1.387	1.385	1.389	1.367	1.398	1.387	1.390	1.389	1.370	1.383	1.388	1.389
N4(N3**)-C(=O)	1.398	1.369	1.370	1.371	1.368	1.343	1.399	1.371	1.390	1.370	1.345	1.373	1.369	1.369
C=O	1.221	1.215	1.214	1.214	1.214	1.231	1.220	1.214	1.231	1.213	1.228	1.215	1.214	1.213
Bond angles(*θ*)														
C2(**C3**,**C4**,**C7**)- C7(C9*)-N2(N1**)	120.8	120.3	120.9	120.8	120.3	120.41	115.6	115.8	117.9	115.3	115.42	120.6	120.6	120.3
C7(C9*)-N2(N1**)-N3(N2**)	116.1	119.7	117.7	117.6	117.9	116.87	116.6	118.4	118.0	118.7	118.44	117.2	117.8	118.0
N2(N1**)-N3(N2**)-C(=O)	118.4	118.4	119.7	119.7	119.6	119.85	117.2	119.2	118.8	118.9	118.72	119.8	119.6	119.4
C(=O)-N4(N3**)- N5(N4**)	116.5	120.6	120.6	120.4	120.80	121.22	116.5	120.5	119.3	120.6	121.43	120.2	120.5	120.5
Dihedral angles														
α	178.3	179.7	179.8	179.7	179.8	-174.73	179.1	179.8	-178.4	-179.0	176.53	179.7	179.7	179.7
B	165.3	175.3	177.7	177.5	177.8	-177.00	171.6	177.4	178.7	178.6	177.51	176.4	177.9	178.2
χ	2.6	1.8	-0.5	-0.7	-0.5	-174.15	7.2	0.7	0	4.1	177.27	-0.2	-1.5	-1.5
δ	8.9	7.8	7.7	7.9	7.2	5.5	9.7	8.0	0	8.3	8.3	8.4	7.4	7.4

* for **8-10;** ** for **1, 2 and 6**; *** crystallographic data used for comparison with the result obtained from theoretical calculation

Table S7. Geometrical data for *Z* isomers of monocarbohydrazones obtained by MP2/6-311G(d,p) method.

Compound/parameter	**1**	**2**	**3**	**6**	**7**	**8**	**9**
Bond distance (A°)							
H-C7(C9*)	1.085	1.088	1.086				
H-N3(N2**)	1.017	1.014	1.023	1.016	1.023	1.013	1.013
H-N4(N3**)	1.011	1.007	1.007	1.011	1.007	1.007	1.008
C2-C7(C9*)	1.477	1.484	1.472	1.487	1.489		
C3-C7						1.493	
C4-C7							1.494
C7-C8				1.500	1.507	1.499	1.498
C7(9*)-N2(N1**)	1.297	1.279	1.283	1.299	1.287	1.277	1.277
N2(N1**)-N3(N2**)	1.372	1.351	1.345	1.375	1.347	1.359	1.360
N3(N2**)-C(=O)	1.399	1.388	1.385	1.394	1.381	1.381	1.382
N4(N3**)-C(=O)	1.397	1.370	1.371	1.400	1.374	1.375	1.374
C=O	1.220	1.214	1.215	1.221	1.216	1.215	1.214
Bond angles(θ)							
C2(**C3**,**C4**,**C7**)- C7(C9*)-N2(N1**)	128.6	127.2	129.9	124.8	127.1	124.2	124.1
C7(C9*)-N2(N1**)-N3(N2**)	117.1	118.3	119.4	116.9	121.1	118.4	118.5
N2(N1**)-N3(N2**)-C(=O)	117.1	119.3	119.0	117.5	118.8	119.5	119.3
C(=O)-N4(N3**)- N5(N4**)	116.7	120.6	120.7	123.5	120.4	120.1	120.1
Dihedral angles (θ)							
α	-0.2	1.9	-0.3	0.6	-0.2	-1.8	0.9
β	165.7	175.9	178.5	165.3	179.5	175.0	175.4
χ	7.8	4.6	-1.2	6.8	-0.5	-1.1	2.4
δ	10.3	8.3	8.1	10.4	9.5	8.5	8.6

** for **2**

MS–MS^n analysis

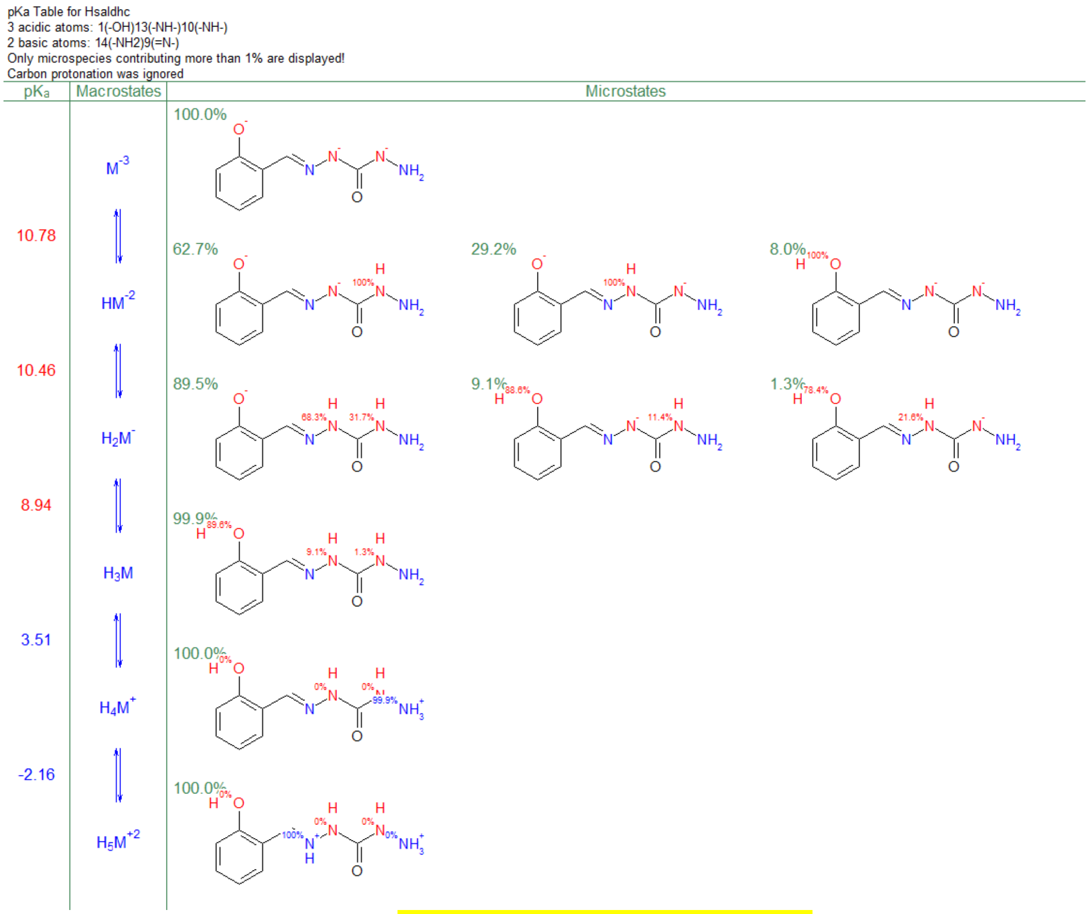

Figure S30 Predicted pK_a values

Fragmentation pattern of studied compounds in positive mode are given on Figs. S31 – S36. General fragmentation paths of compound **2** is given on Fig. S20. In MS spectrum of the compound **2** ($C_8H_{10}N_4O_2$, exact mass is 194.08) the base signal at *m/z* = 195.12 was assigned to protonated molecular ion, $[M + H]^+$. The signal of sodium adduct, $[M + Na]^+$ appeared at *m/z* = 217.02, and similar sodium adducts with molecular ions of other investigated compounds were found 121.92 *m/z* values. Fragment at *m/z* 162.92 was obtained by elimination of hydrazine (Fig. S31; **2-I$_a$**) and is further fragmented by losing hydroxyl radical and CONH fragment producing 2-(2-hydroxybenzylidene)-1-methylidenehydrazinium ion, observed at *m/z* 145.92 (**2-I$_b$**’) and ion at *m/z* value 119.92 (**2-I$_b$**”), respectively. Stepwise loss of semicarbazide, i.e. $H_2NNHCONH_2$ from $[M+H]^+$ ion, gave *m/z* 121.92 ion, from which lose the hydrogen cyanide and water, produce protonated phenol, *m/z* 94.83 (**2-III$_b$**), and phenyl cation, *m/z* 76.92 (**2-III$_c$**), respectively. The loss of the carbonyl hydrazine (aminoisocyanate), H_2NNCO, group from the $[M+H]^+$ ion produced the third fragment found in the MS^2 spectrum of the compound **2** at the *m/z* 136.92. This ion was further fragmented by losing the ammonia producing ion at *m/z* 119.83 in MS^3 spectra. Further fragmentation trough the loss of the hydrogen cyanide and consecutive loss of carbon monoxide reveals ions *m/z* 92.83 (**2-II$_c$**) and 64.75 (**2-II$_d$**), respectively.

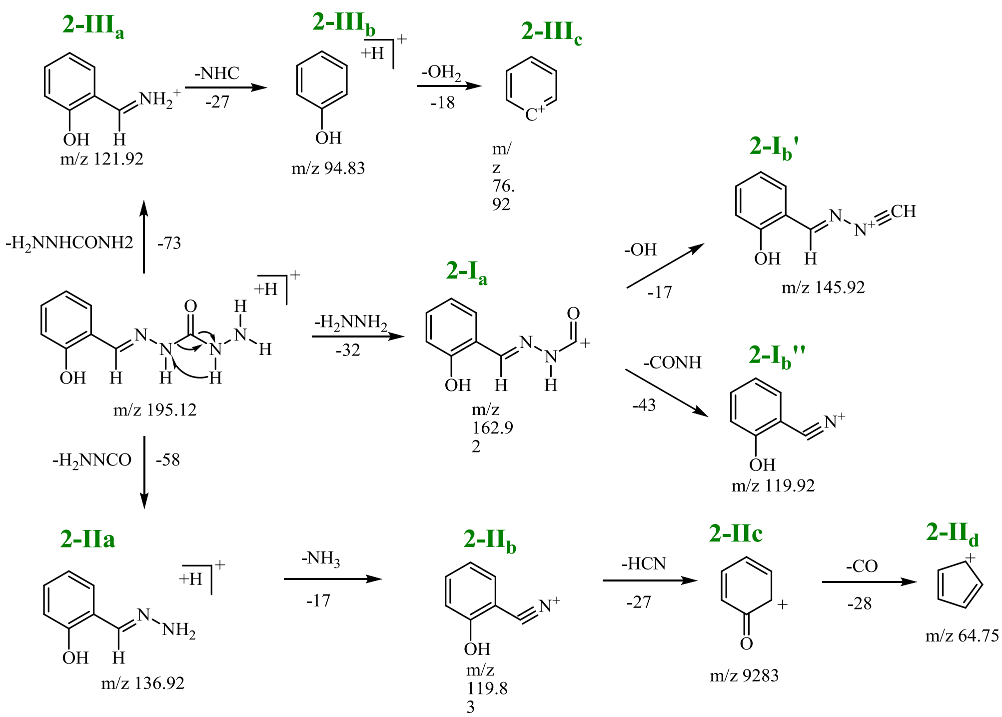

Figure S31**.** Fragmentation pattern of protonated molecular ion $[\mathbf{2}+H]^+$ (m/z = 195.12)

Fragmentation pathways of compounds **1**, **3-5** in positive mode are given on Fig. S32. For the compounds **1** and **3-5** first fragmentation step was similar to the fragmentation of the compound **2**. The main fragmentation path, which was common for all four compounds was the elimination of hydrazine in the first step (**1**, **3**-5-**I$_a$**), in the second step, elimination of CO (**1**, **3-5-I$_b$**) and in the third step elimination of nitrogen (**1**,**3**-5-I$_c$). The last fragmentation step, in which hydrogen cyanide was detached, was only possible for **3-5-I$_c$** fragmetns and **3-5-I$_d$** ions, *i.e*. cyclopentadienil cation, was obtained. All four compounds by losing the –H_2NNCO group formed a second ion in MS^2 spectra (1,3-5-II$_a$) which was only in the case of the compound **5** stable enough to be further fragmented (**1**, **3-5 -X$_a$**)

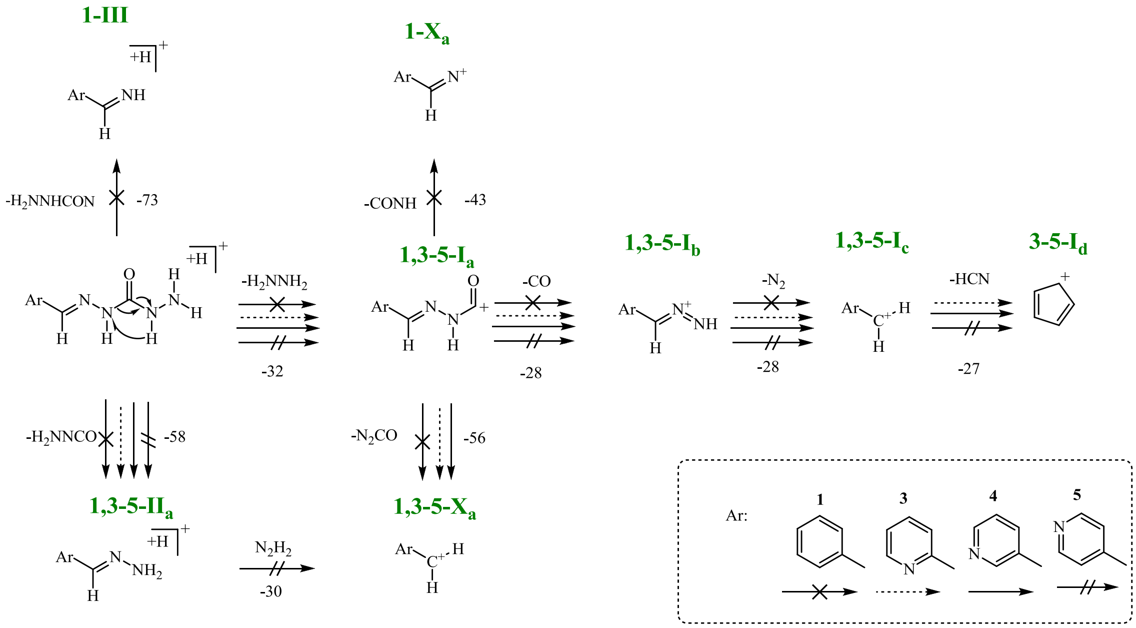

Figure S32. Fragmentation pattern of protonated molecular ion [**1**, **3**, **4** and **5**+H]$^+$ (*m/z* = 179,03 and 180.11)

For compounds **6-9,** fragmentation behavior was similar to the fragmentation obtained for the compounds **1** and **3-5**. Common fragmentation scheme for the compounds **6-9** is presented at the Fig. S33. For all three compounds common fragmentation path (and for **9** only fragmentation path) was elimination of hydrazine in the first step (**6-9-I$_a$**), in the second step, elimination of the CO (**6-9-I$_b$**) and in the third step elimination of nitrogen led to the formation of 1-(pyridin-3-yl)ethane-1-ylium ion (**6-9-I$_c$**). For the compounds **6**, **7** and **8** fragmentation of the [M+H]$^+$ ion reveals 3-(1-hydrazinoethyl)pyridine ion, produced by the loss NH_2NCO (aminoisocyanate) group (**6-8-II$_a$**). Subsequent fragmentations, in the case of compound **8**, lead to the formation of $ArC_2H_3N^+$ ion by the loss of the ammonia (**6-8-X$_a$**). For the compounds **6** and **7** the same ion was generated in MS^3 spectrum but trough different fragmentation path, *i.e.* by losing –CONH group from **6-9-I$_a$** ion. Subsequent fragmentation of $ArC_2H_3N^+$ yielded two final fragments by losing the hydrogen cyanide (**6-8-X$_a$'**) and $NCCH_2$ (**7-8-X$_b$''**). For compounds **6** and **8** the third fragment was found in the MS^2 spectrum obtained by loosing the –$H_2NNHCON$ group. Further fragmentation of these ions was not possible.

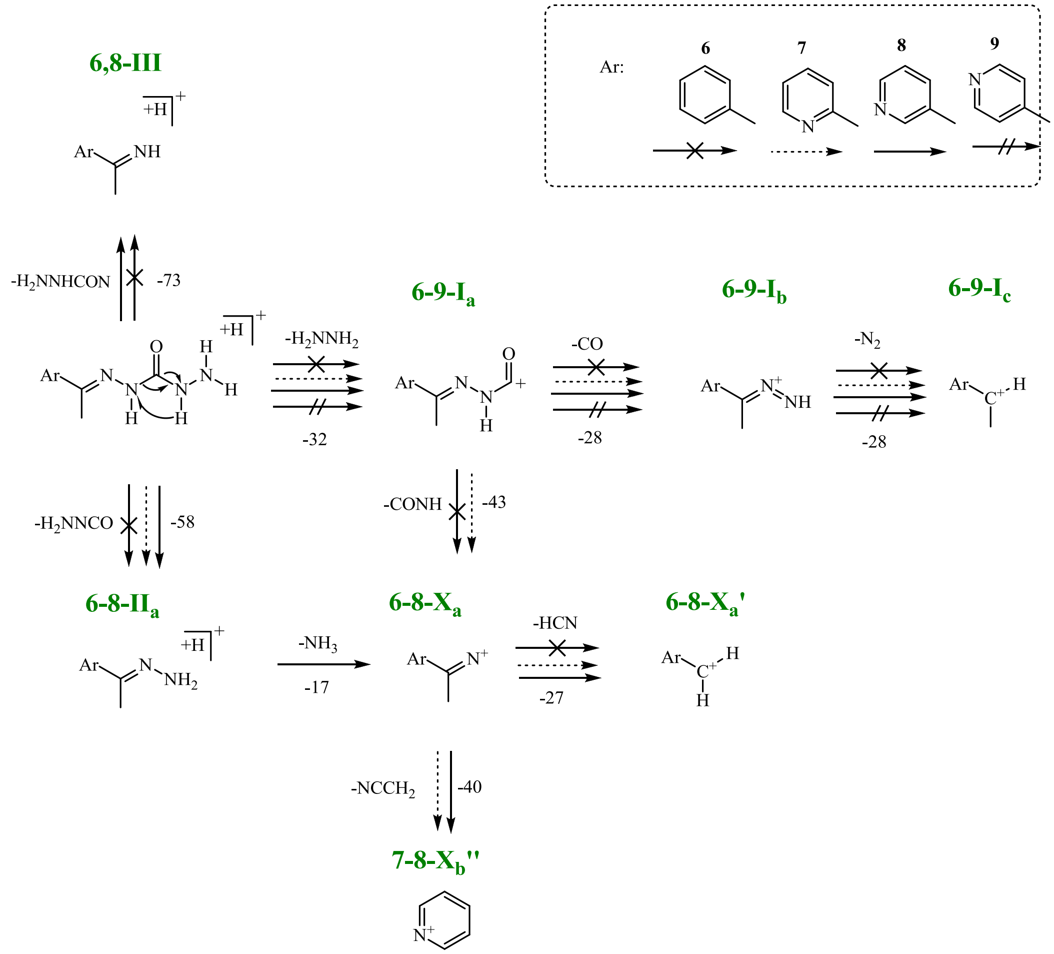

Figure S33. Fragmentation pattern of protonated molecular ion [**6 - 9**+H]$^+$ (m/z = 194.07 and 194.14)

Fragmentation scheme for the compound **10** is presented at Fig. S34. MS^2 spectrum reveals one fragment at *m/z* 198 which is subsequently fragmented producing three fragments at *m/z* 141.92, 154.92 and 181.00. The most abundant fragment at the *m/z* 141.92 was further fragmented to the 7*H*-cyclopenta[*b*]pyridin-7-ylium ion (**10-I$_b$'**). Fragment at the *m/z* 154.92 by losing the hydrogen cyanide produced quninolinium cation at the *m/z* 127.83 (**10-I$_c$)**, and the least abundant fragment at the *m/z* 181.00 by losing the H_3CN group generated quinoline-7-carbonitrile at *m/z* 152.92 (**10-I$_b$')**.

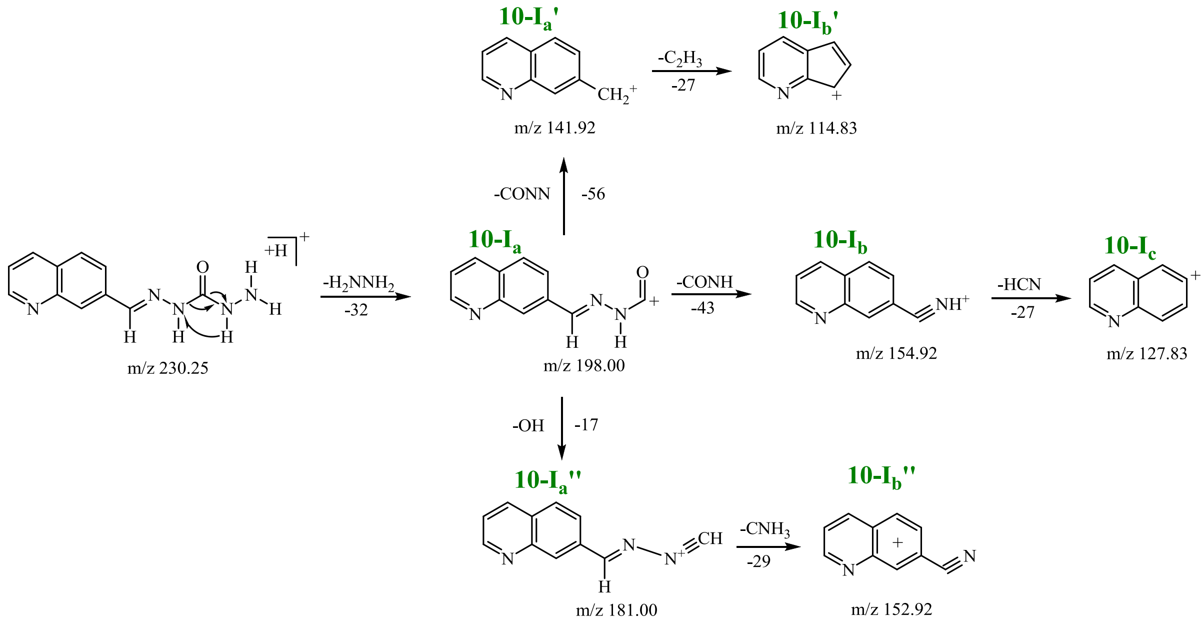

Figure S34. Fragmentation pattern of protonated molecular ion [**10**+H]$^+$ (*m*/*z* = 230.25)

Fragmentation pattern of protonated molecular ions **[11** and **12**+H]$^+$ are given on Fig. S35. Compunds **11** and **12** displayed very similar fragmentation behavior to the compounds **3-5**. Both of the compounds in the first fragmentation step formed a fragment by losing carbonyl hydrazine group (**11-12-I$_a$**), after which was followed by the loss of CO (**11-12-I$_b$**) and N_2 (**11-12-I$_c$**). The final fragmentation step performed for the ion Ar-CH_2^+ resulted in the formation of ion at *m/z* 114.83 and *m/z* 130.17 for the compounds **11** and **12**, respectively. For the compound **11** another fragment, observed at the *m/z* 172.17, was obtained in the first fragmentation step.

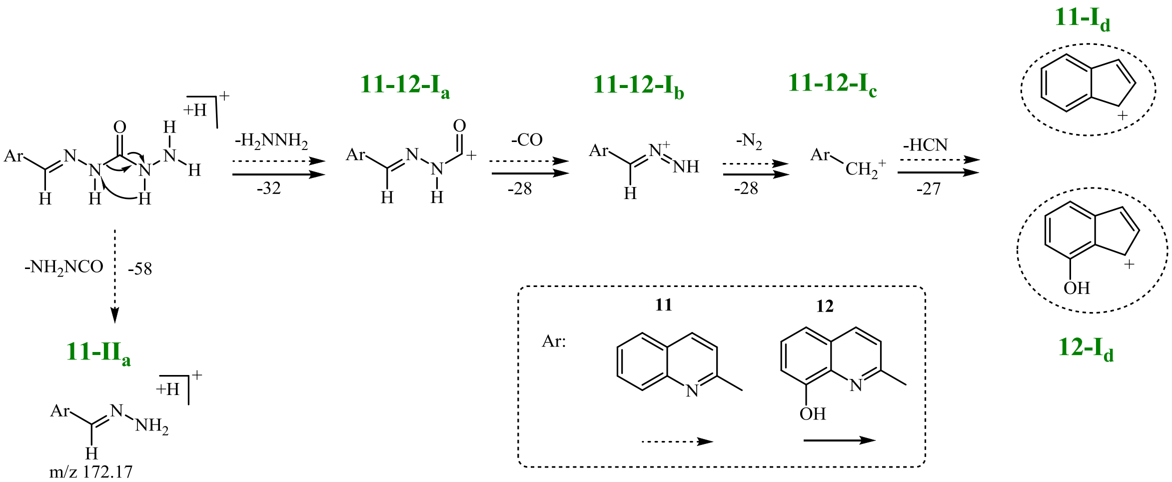

Figure S35**.** Fragmentation pattern of protonated molecular ions **[11** and **12**+H]$^+$

(m/z = 246.04 and 230.25)

Fragmentation pattern of compound **1 - 12** in negative mode are given on Fig. S36. Compounds **5**, **8** and **9** were further fragmented producing the ions presented as **5** and **8-I$_c$** and **9-I$_d$** at Fig. S23, respectively. In the first fragmentation step compounds **2** and **12**, beside the loss of the NHNHCO group, generated a fragment by the loss of H_2NNH_2 group (**2** and **12-II$_a$**). The third fragment in the first fragmentation step was obtained for the compounds **3** and **10** generated by the loss of the $NHNHCON_2$ group.

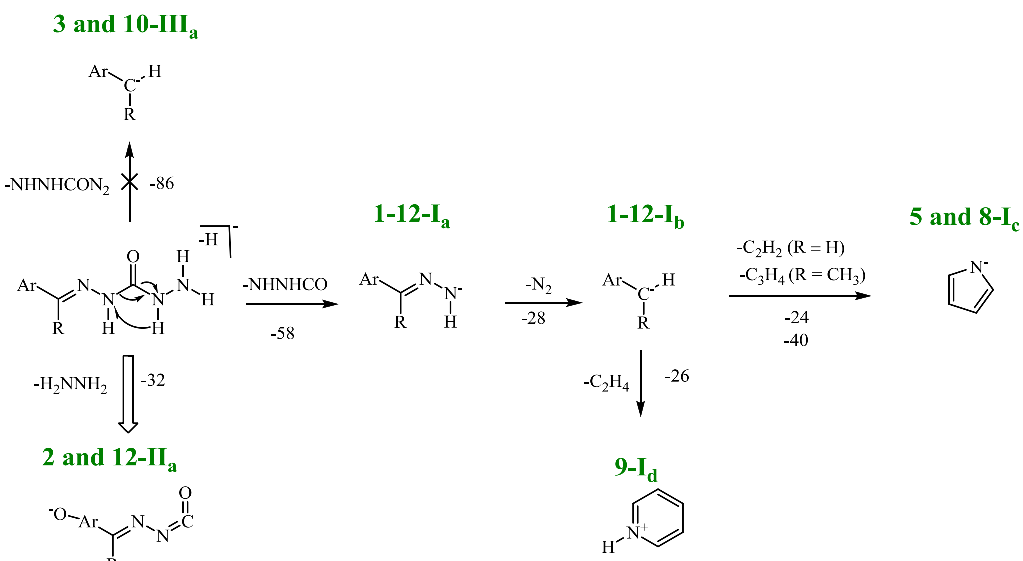

Figure S36. Fragmentation pattern of deprotonated molecular ions [**1 - 12**-H]$^-$

3.2 Spectral properties of mCHs

The aim of this study was to experimentally analyze structure of mCHs, and to provide theoretical explanations with the aid of molecular modelling and LF(S)ER analysis. Experiments were oriented toward determination of solution and solid state structures, taking into account conformation, isomerization, and tautomerism. As a result, numerous fundamental molecular properties could be obtained as a base for the establishment of quantitative structure-properties relationships (QSPRs). Such findings are the basics for the rational design and property predictions of novel compounds.

One of the experimental techniques used in this study was UV-Vis spectroscopy. This simple technique is valuable method frequently used for for studying of spectral properties of the tautomeric forms and conformational isomer, electronic structure in the course of transition, isomerisation and tautomeric equilibria, sensitivity of the tautomeric equilibria and isomerization processes to solvent dipolarity/polarizability, basicity and acidity, as well as substituent effect. The solvatochromism relate to the change in position of a UV-Vis absorption band that accompanies a change in solvent polarity. Spectral behavior of studied compounds could be described by electronic structure in both ground and excited states induced by change of a solvent properties. It was confirmed that more planar structure produce larger bathochromic shift due to the increased of π-conjugation (Rančić et al., 2016). The bathochromic shift (red shift or positive solvatochromism) is associated generally with increased solvent polarity, and basically it is caused by the difference in stabilization of the electronic structure between the ground and excited state. In general, the understanding of the solvent effect on absorption spectra, from the experimental and theoretical aspect, is of particular importance for deeper insight into QSPR analysis when chemical properties are modeled as the response variable.

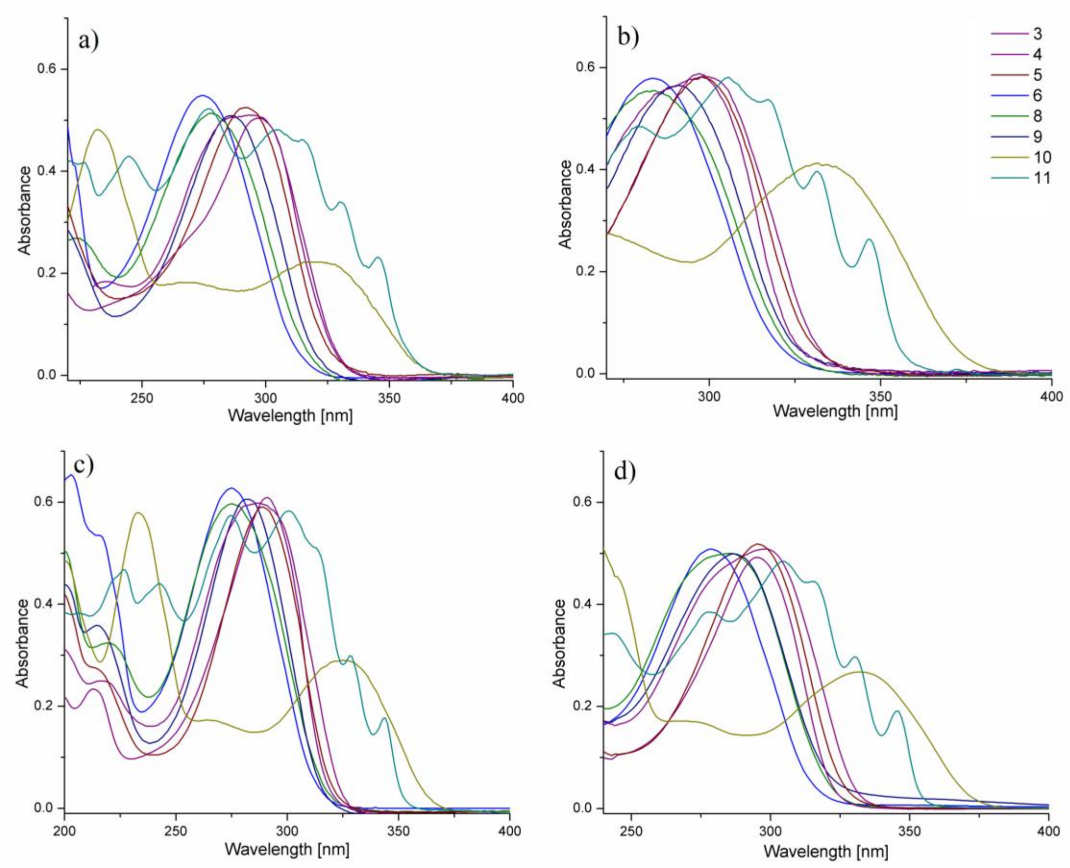

Figure S37. Absorption spectra of compounds **3–6** and **8-11** in a) EtOH, b) DMSO, c) AcN and d) THF.

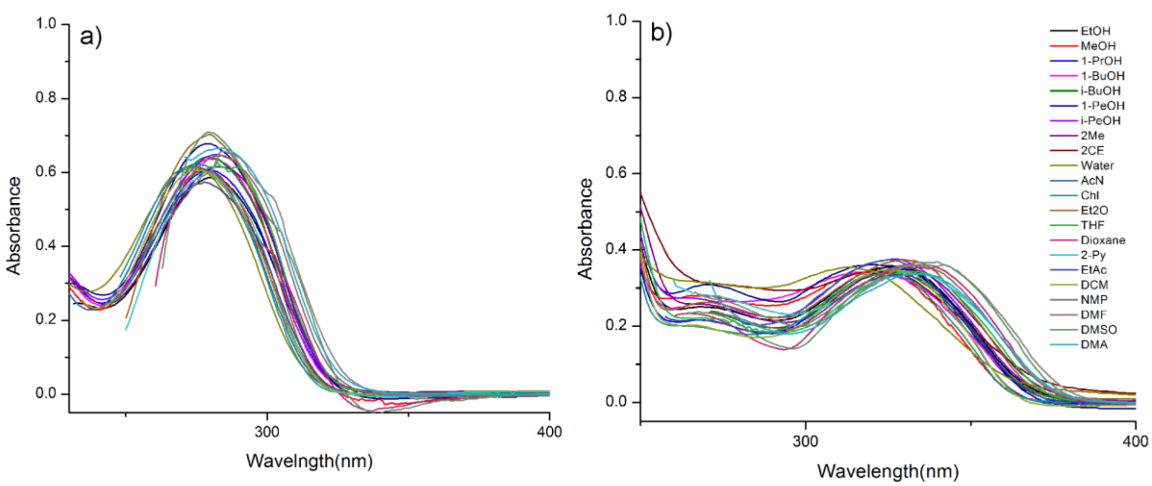

Figure S38. The UV-Vis spectra of selected compounds a) **4** and b) **10** in all solvents tested

3.3. Dependence of compound solvatochromism on its structure

Correlation results in Table S8 indicate complex influences of both solvent and substituent effects on absorption maxima change reflected in large variation of the contribution of non-specific and specific solvents effects to UV-Vis spectral shifts. In general lower sensitivity to solvent effects was found for compound **2** with respect to **1** and **6**, considering electronic and structural effects of the substituent at azomethine carbon. These results suggest higher stabilization of compound **2** due to formation of six membered pseudo cyclic hydrogen bridge while introduction of methyl group cause appropriate out-of-plane rotation, and thus higher contribution of non-specific solvent effect is a consequence. The negative sign of coefficients *s* and *b* for all mCHs indicates batochromic shift of ν_{max} with increasing solvent dipolarity/polarizability and hydrogen-bond accepting capability. These results suggest better stabilization of the electronic excited state relative to ground state. The highest value of coefficients *s* and *b* were found for compound **9**, and somewhat lower value of coefficient *s* were found for compounds **4**, **6** and **8**. These results indicate that both electron-accepting properties of 3- and 4-pyridyl groups in compound **4**, **8** and **9** together with steric interactions of methyl group contribute to higher solvent/solute dipolarity/polarizability interactions. Similar behavior of two series of mCHs: **3-5** and **7-9**, showed substituent dependent effect from the position of "aza" group and steric effect of azomethine methyl group. Different behavior showed compounds **10-12** where "aza" in 2-position deviate from linear realtion. Low values of correlation coefficients reflect effect of higher stability of quinoline based structure.

The positive sign and lower values of coefficient *a* for all compounds (Table S8), except for compounds **9** and **11** (Table S8), indicates a hypsochromic (blue) shift relative to increased solvent hydrogen-bond donating capability. This suggests better stabilization of the ground state relative to the excited state. The highest value for coefficient *a* was found for compound **10** (0.86; Table S8).

Table S8. Results of the correlation analysis for E isomers according to Kamlet–Taft equation.

Comp.	$\nu_0\times10^{-3}$ (cm^{-1})	s×10^{-3} (cm^{-1})	b×10^{-3} (cm^{-1})	a×10^{-3} (cm^{-1})	R[a]	Sd[b]	F[c]	Solvent excluded from correlation[d]
1	34.80 ±0.11	–0.50 ±0.14	–0.78 ±0.12	0.53 ±0.08	0.96	0.1	50.60	*2CE, DCM, H_2O, AcN, 2ME, Dioxan*
2	31.46 ±0.11	–0.11 ±0.14	–0.41 ±0.07	+0.29 ±0.07	0.93	0.06	23.36	*H_2O, Chl, AcN, EtAc, DMA, 2-Py, THF, Et_2O*
3	34.03 ±0.09	–0.44 ±0.12	–0.19 ±0.33	+0.34 ±0.05	0.94	0.09	34.42	*H_2O, DCM, 2ME, AcN, DMA, 1-BuOH*
4	34.59 ±0.19	–1.26 ±0.25	–0.59 ±0.14	+0.19 ±0.11	0.93	0.15	27.13	*H_2O, DMA, AcN, Et_2O, DCM*
5	35.09 ±0.22	–0.73 ±0.26	–1.18 ±0.14	–[e]	0.95	0.12	31.27	*H_2O, 2ME, DCM, EtAc, AcN, Et_2O, THF*
6	37.02 ±0.17	–1.25 ±0.23	–0.46 ±0.16	+0.46 ±0.11	0.94	0.17	36.97	*Dioxan, H_2O, AcN, DCM*
7	34.76 ±0.15	–0.70 ±0.17	–0.55 ±0.12	+0.44 ±0.10	0.94	0.12	30.77	*H_2O, 2CE, 2ME, THF, Dioxan*
8	36.08 ±0.10	–1.11 ±0.22	–0.51 ±0.16	+0.023 ±0.14	0.92	0.15	20.00	*H_2O, MeOH, AcN, DCM, THF, 2CE, 1-PeOH*
9	36.67 ±0.20	–1.51 ±0.21	–1.43 ±0.19	–0.27 ±0.11	0.95	0.14	36.45	*H_2O, DCM, Dioxan, 2ME, EtAc, 2-Py*
10	30.68 ±0.14	–0.18 ±0.18	–0.92 ±0.12	+0.86 ±0.10	0.95	0.13	41.13	*H_2O, 2CE, 2-Py, AcN*
11	33.38 ±0.07	–0.87 ±0.09	–0.11 ±0.07	–0.34 ±0.10	0.95	0.07	40.19	*AcN, H_2O, MeOH, 2ME, EtOH*
12	31.018 ±0.18	–0.43 ±0.22	–0.69 ±0.11	+0.44 ±0.11	0.94	0.11	23.89	*H_2O, 2CE, AcN, Dioxan, NMP, Et_2O,2-Py, 2ME*

[a] Correlation coefficient; [b] Standard deviation; [c] Fisher test of significance; [d] abbreviation for the solvents are given in Table S2; [e] negligible value

3.4. LFER analysis of of UV-Vis and NMR data

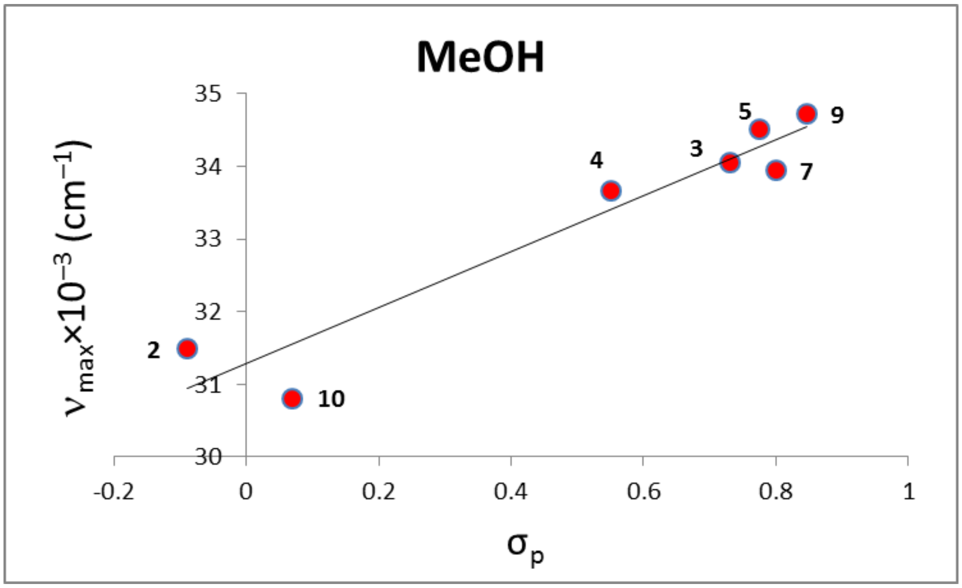

a)

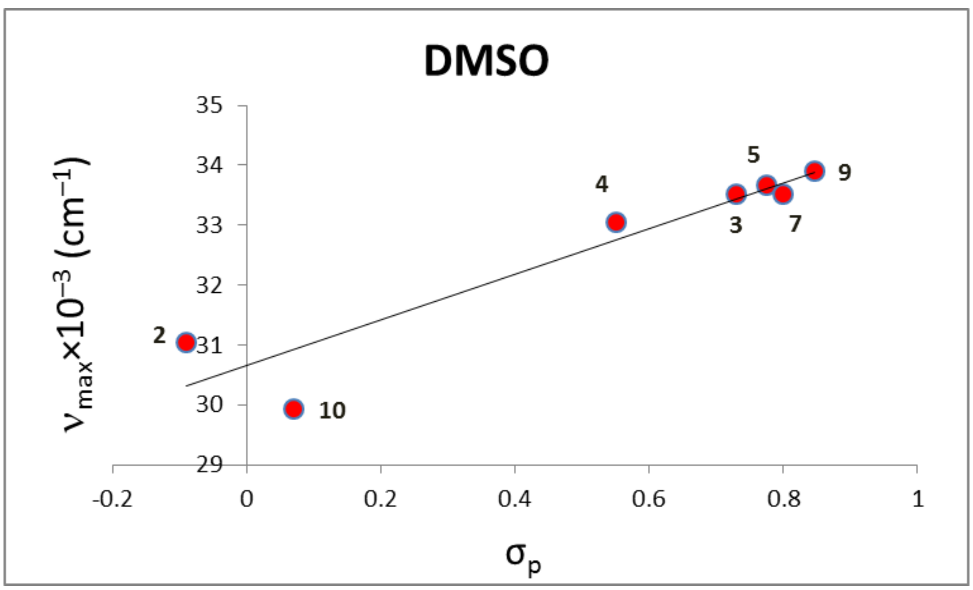

b)

Figure S39. Results of LFER correlations of the UV-Vis data of mCHs with σ constants using Hammett Eq. (3) in: (**a**) MeOH, **b**) DMSO for mCHs in *E* form.

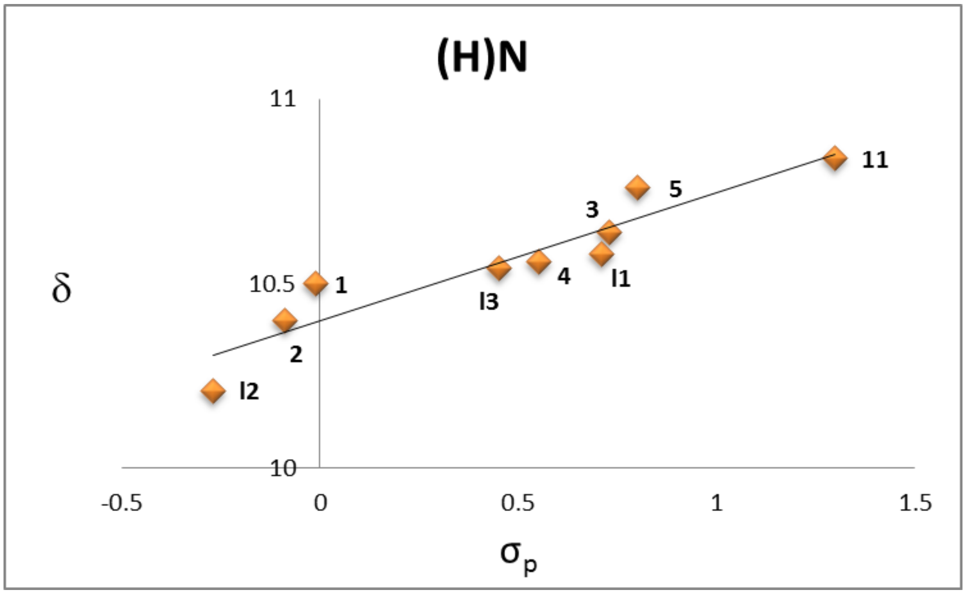

a)

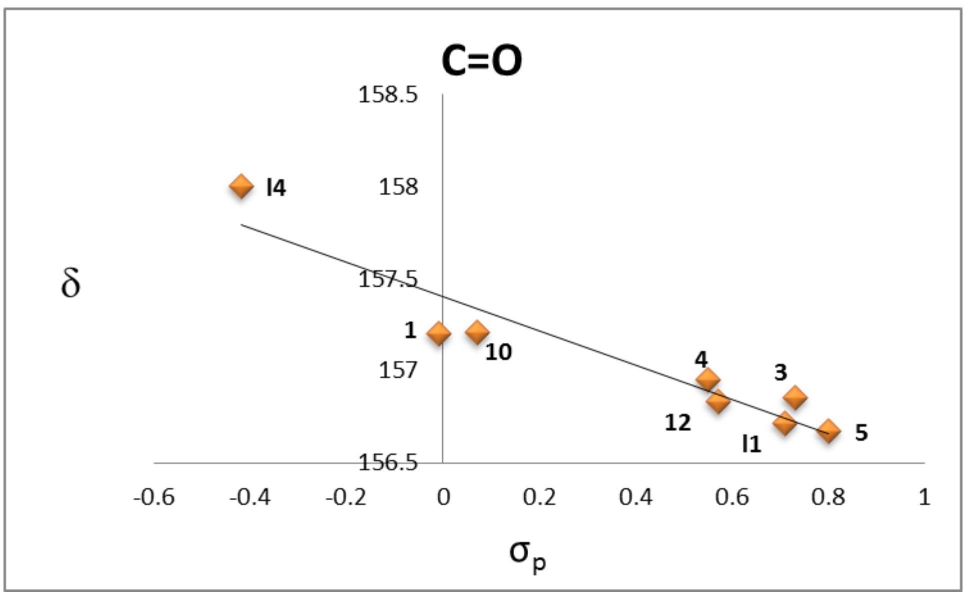

b)

Figure S40. Results of LFER correlations of the NMR data of mCHs with σ constants using Hammett Eq. (3) for (H)N (**a**) and C=O **b**) of carbohydrazones in *E* form

The field effect, induced by substituent dipole, causes subsidiary polarization of π-electrons in the subsequent independent π-electronic system without net π-electron transfer. According to Reynolds (Reynolds et al., 1983), the polar effect mainly arises as a result of the substituent dipole induced field effect, and this effect alters the electron density at C5 by two mechanisms: (*i*) field-induced polarization of the side chain vinyl group (localized or direct $\pi-$ polarization), and (*ii*) field-induced $\pi-$ electron transfer (extended $\pi-$ polarization) (Rančić et al., 2013). The second term is major effect operative mostly in planar systems. Reynolds' conclusion that the polar effect is of field, rather than inductive origin, is supported by the observation that its influence on C5 is approximately the same from the *meta–* and *para–* positions (Craik and Brownlee, 1983; Reynolds et al., 1983). The resonance interaction in the extended conjugated system of the substituted styrene molecules in the presence of electron– acceptor substituent has complementary effect to the polarization mechanism and the opposite is true for electron-donor substituted compounds.

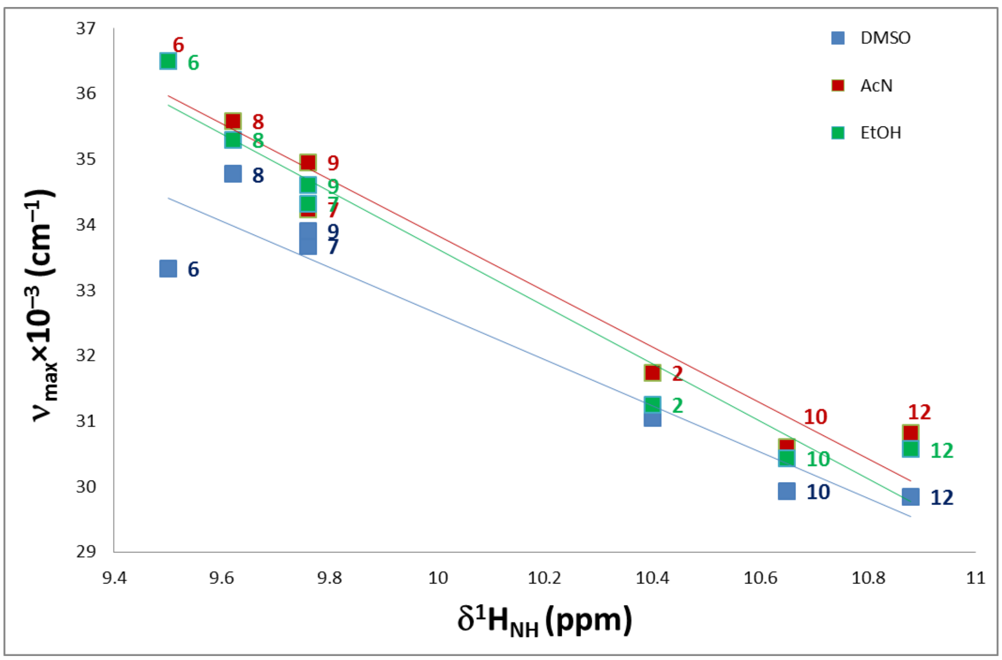

Figure S41. Correlation plot of ν_{max} of compounds **2**, **6, 7, 8, 9, 10** and **12** in DMSO, AcN and EtOH *versus* ^{1}H NMR of N-H chemical shifts recorded in DMSO-d_6

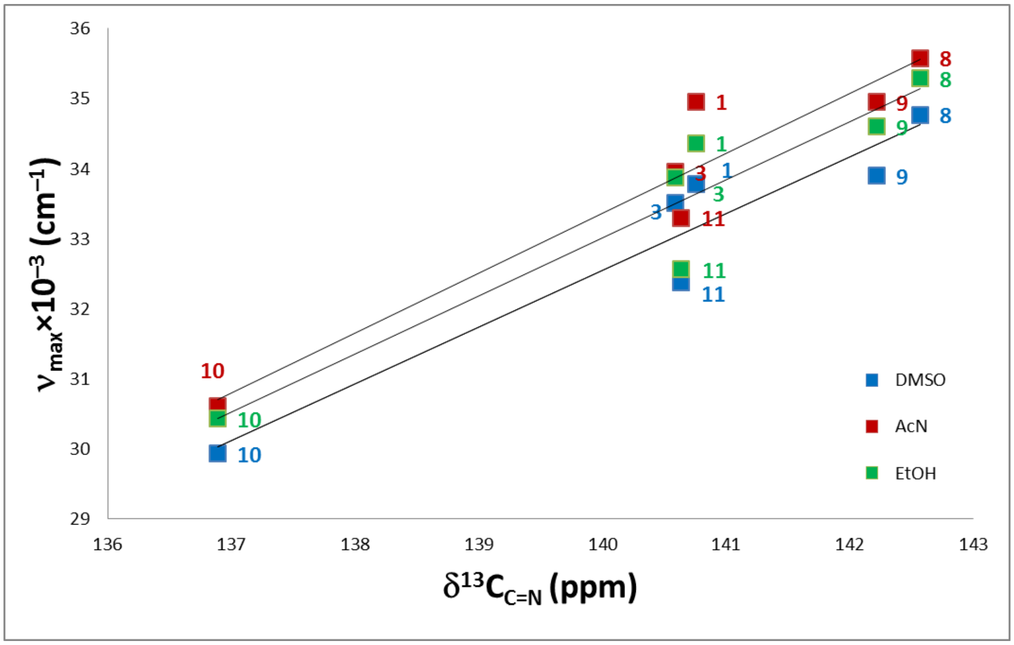

Figure S42. Correlation plot of ν_{max} of compounds **1**, **3**, **8**, **9**, **10** and **11** in DMSO, AcN and EtOH *versus* ^{13}C NMR of azomethine carbon (C=N) chemical shifts recorded in DMSO-d_6

3.5 Photochromism of carbohydrazones

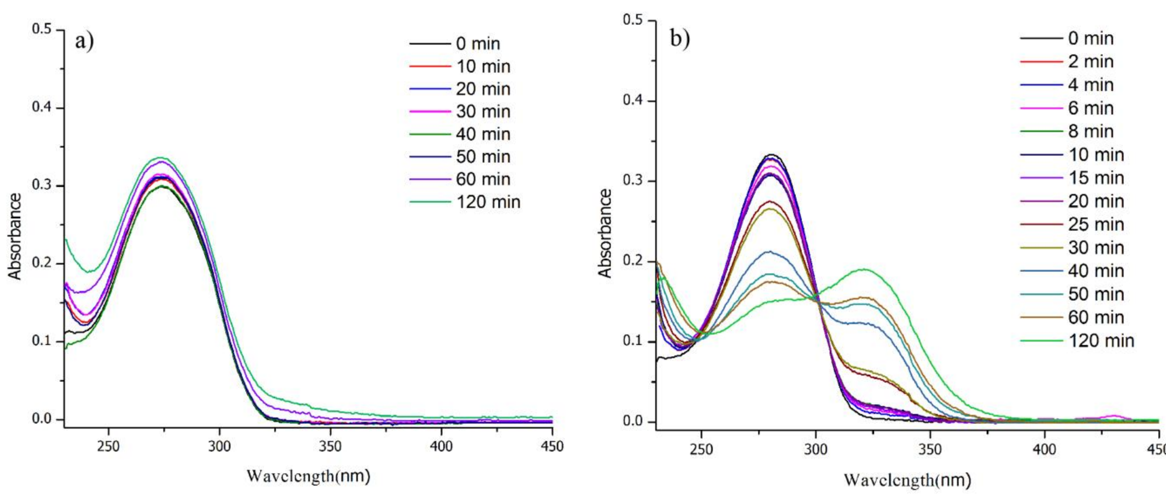

Figure S43. Evolution of UV absorption spectra during the irradiation of compounds **8** (a) and **9** (b) (1.0×10^{-5} mol L^{-1}) in DCM

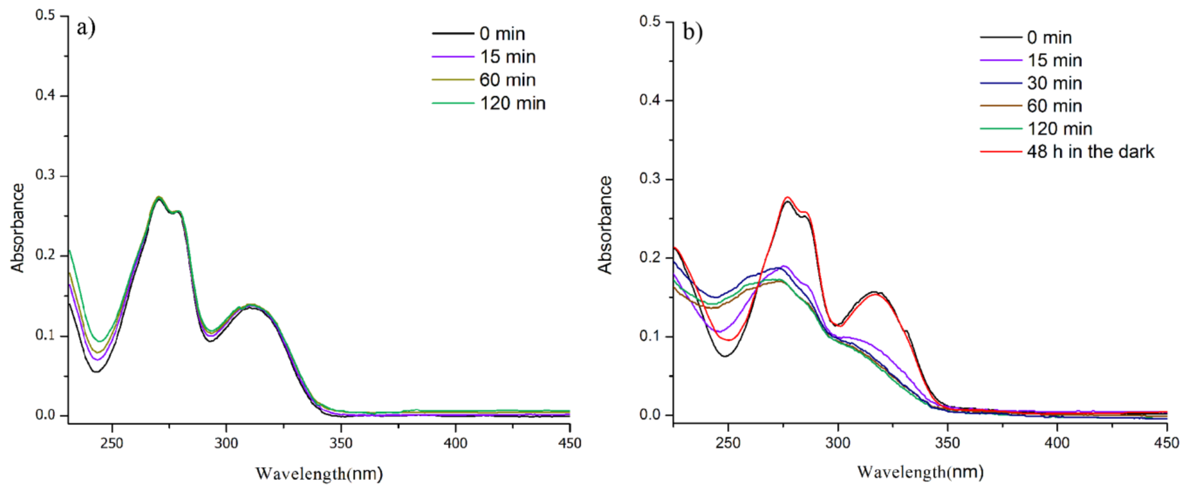

Figure S44. Evolution of UV absorption spectra during the irradiation of compound **2** (1.0×10^{-5} mol L^{-1}) in DCM (a) and MeOH (b)

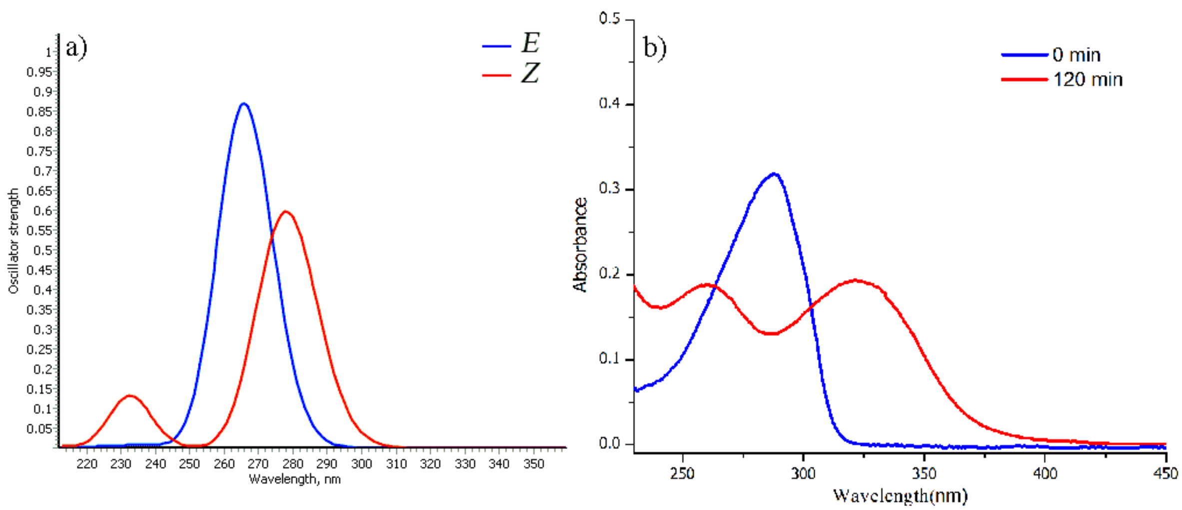

Figure S45. Theoretical a) and experimental spectra b) obtained before and after UV irradiation of compound **7** in *E* and *Z* forms

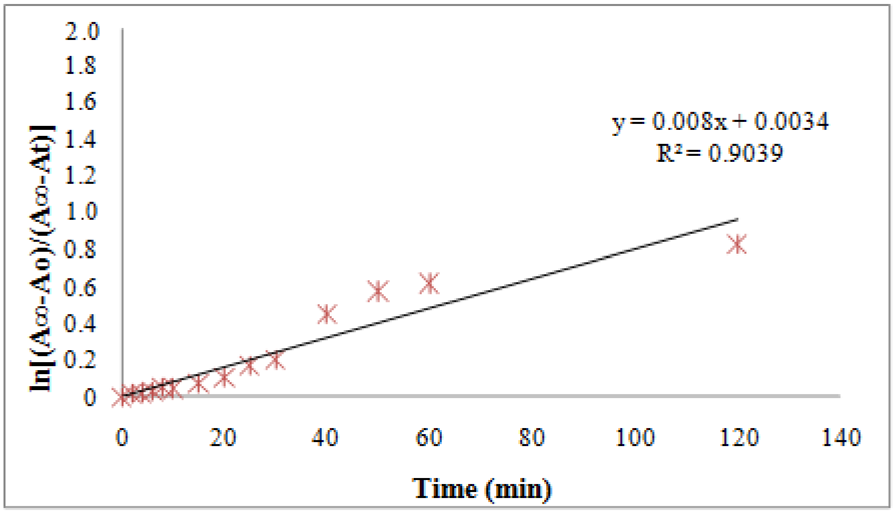

Figure S46. Plot of $\ln[(A_\infty - A_0)/(A_\infty - A_t)]$ with time for the photocoloration reaction of compound **9** under 364 nm light irradiation, where A_0, A_∞ and A_t are the observed absorption data corresponding to 364 nm wavelength in DCM at time zero, infinite time, and time t of the reaction, respectively.

Table S9. Results of ωB97X-D/6-311G(d,p) and AIM calculations of investigated compounds **2**, **3** and **7** in MeOH

Comp.	Tautomer	Energy (kcal)	N---H (Å)	ρ	$\nabla^2\rho$	μ (D)
2	*E*	0.0	1.764	0.0454	0.117	6.9343
	Z	11.56				4.8235
3	*E*	1.73				2.6263
	Z	0.0	1.906	0.0348	0.108	8.2079
7	*E*	0.62				3.1011
	Z	0.0	1.846	0.0399	0.119	8.3915

3.6 Acidity constant determination

Chemical properties of organic molecules in solution depend largely on the degree of ionization, *i.e.* their capability to release/accept proton in aqueous solutions. Proton transfer most frequently occurs between proton-donating/accepting sites at water molecule and any hydrogen-containing (ionizable) atom present in studied molecule. The protonation/-

deprotonation processes depend significantly on the ionization potential of the site disturbed by proton transfer. Overall/local charge distribution in the molecule also sensitively changes/varies with protonation/-deprotonation of the acid/base active sites, respectively, and the easeness of proton acceptance/donation is determined by the thermodynamical stability of conjugated acid (base).

Nitrogen atoms of the hydrazone group are nucleophilic, although the amino type nitrogen is more reactive than urea (amido) nitrogens. The carbonyl group has both electrophilic and nucleophilic character. Imino nitrogen, due to conjugation with aromatic moiety, contributes to increased electrophilic character of imine carbon with low hydrogen accepting ability. Thus measurement of protonation-deprotonation process reflects charge distribution change (both local and at longer distance from the active site), and it can be evaluated by pK_a determination experimentally and compared to predicted values (ADMET Predictor, 2015) to confirm successfulness of applied experimental methodology.

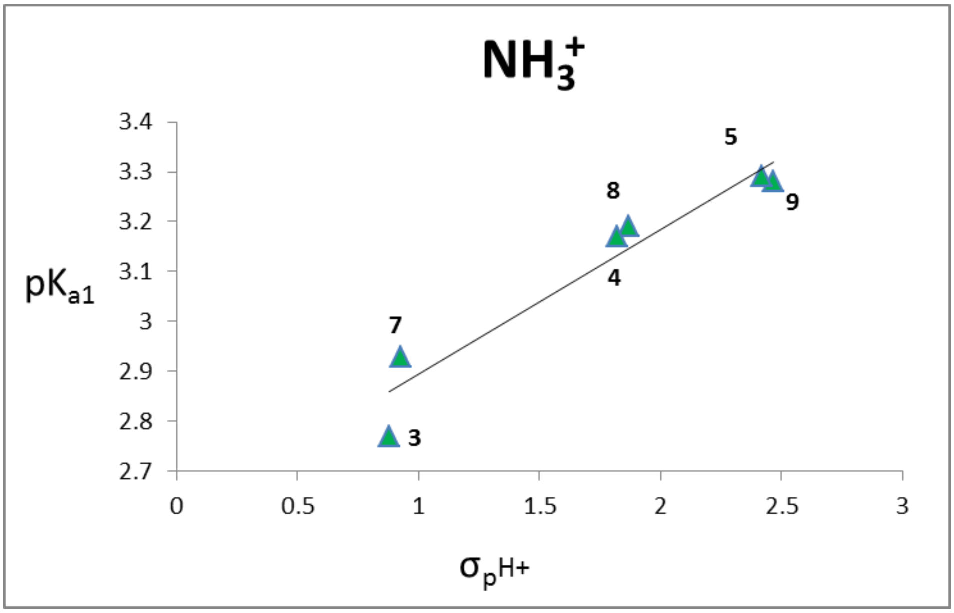

a)

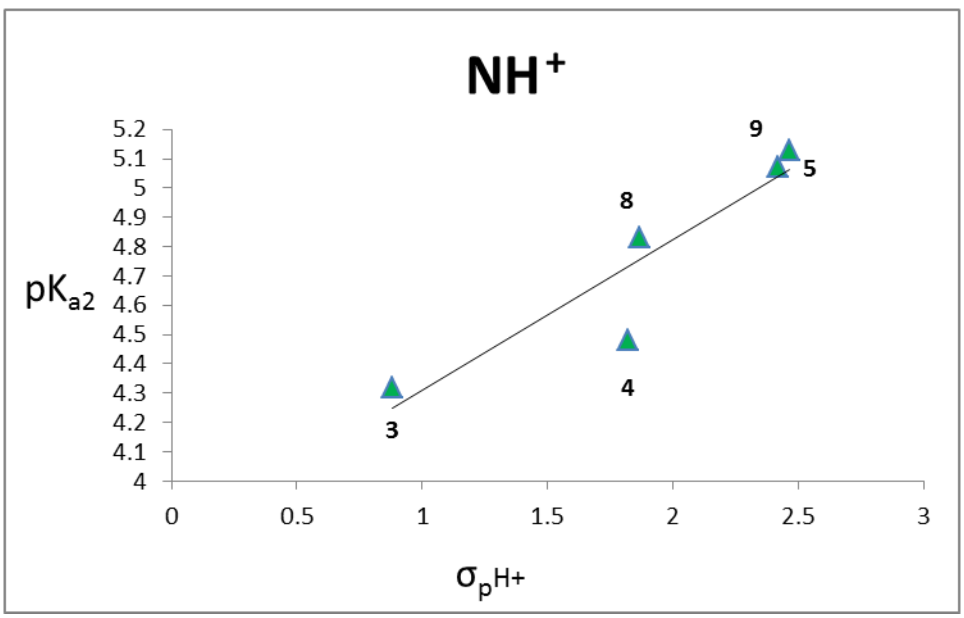

b)

Figure S47. Correlation results of the pK_a values of mCHs with σ_{pH+} constants using Hammett Eq. (3): (**a**) (pK_{a1})NH_3^+, **b**) (pK_{a2})NH+(OH)

3.7. TD-DFT calculations: nature of the frontier molecular orbitals and quantification of ICT

Table S10. Calculated energies of the HOMO and LUMO orbitals and energy gaps for investigated compounds in DMSO.

Comp.	E_{HOMO}	E_{LUMO}	E_{gap}
1 / *E*	-7.648	-0.421	7.227
1 / Z	-8.015	-0.224	7.791
2 / *E*	-7.991	0.301	8.292
2 / Z	-8.442	0.613	9.055
3 / E	-8.362	0.101	8.462
3 / Z	-8.371	-0.058	8.313
4 / E	-8.320	0.089	8.409
5 / E	-8.526	-0.088	8.438
6 / E	-7.656	-0.174	7.428
6 / Z	-7.975	0.134	8.109
7 / E	-8.253	0.238	8.491
7 / Z	-8.244	0.043	8.287
8 / E	-8.298	0.308	8.606
8 / Z	-8.612	0.670	9.282
9 / E	-8.459	0.099	8.558
9 / Z	-8.665	0.502	9.168
10 / E	-7.953	-0.343	7.610
11 / E	-8.261	-0.300	7.961
12 / E	-7.941	-0.310	7.630

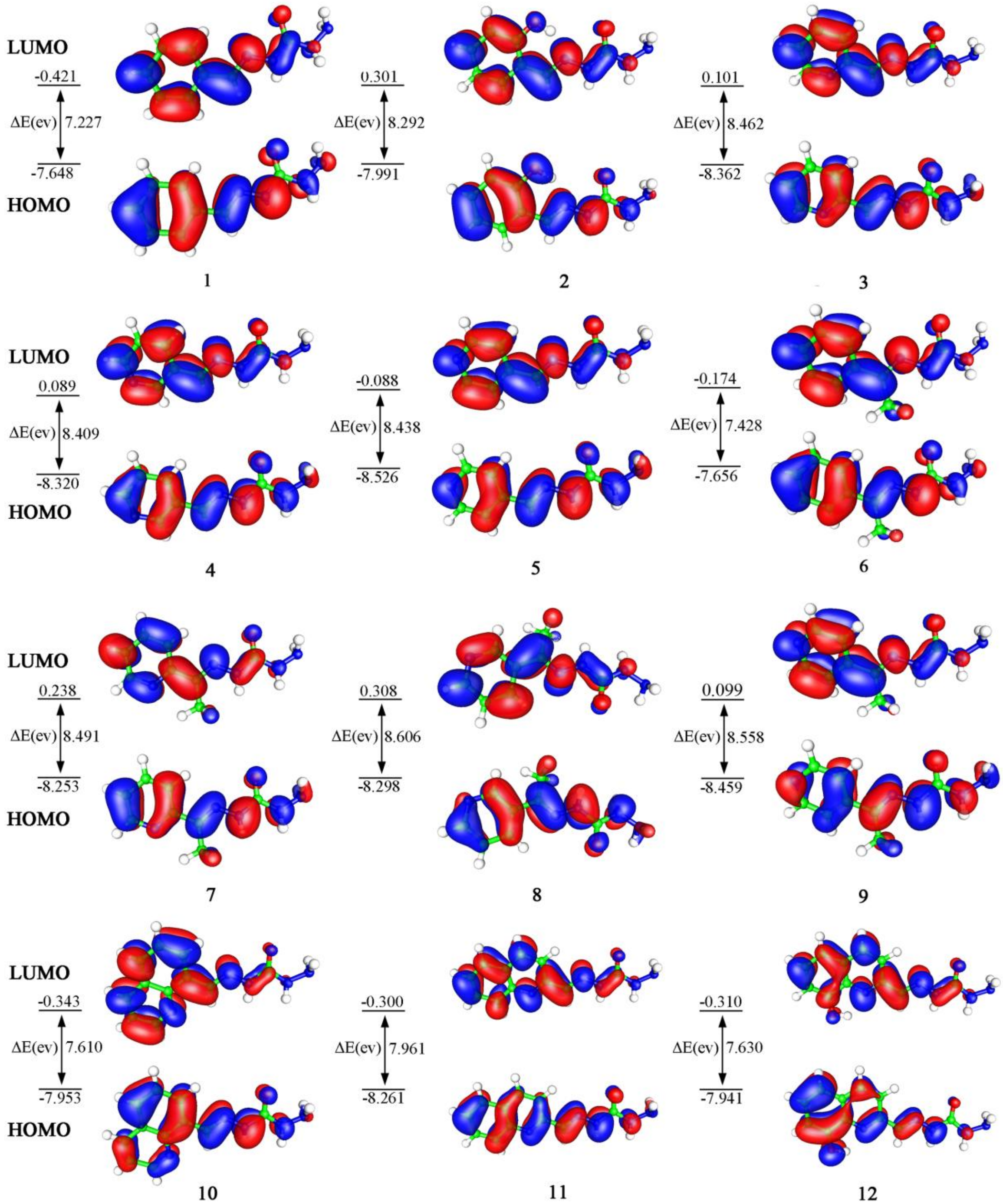

Figure S48. The HOMO/LUMO orbitals and E_{gap} of compounds **1- 12** in *E* form in DMSO

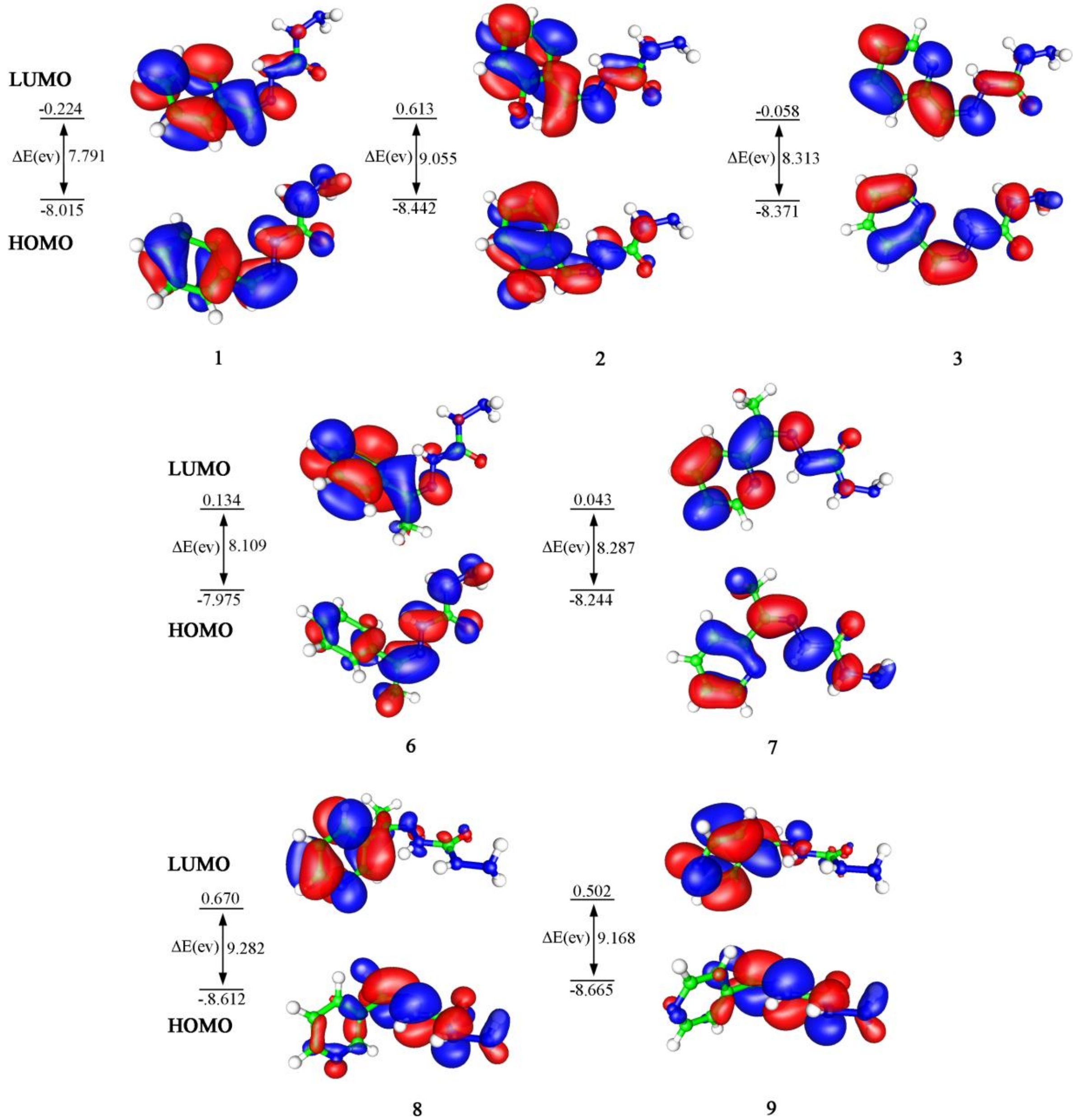

Figure S49. The HOMO/LUMO orbitals and E_{gap} of compounds **1- 3** and **6-9** in *Z* form in DMSO

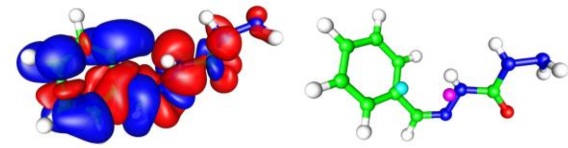

1

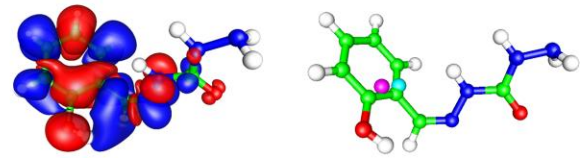

2

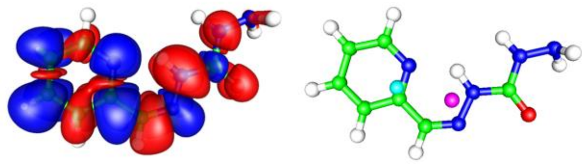

3

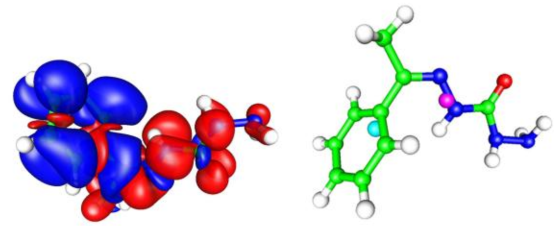

6

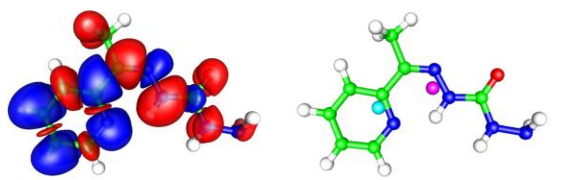

7

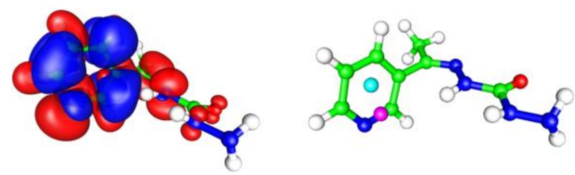

8

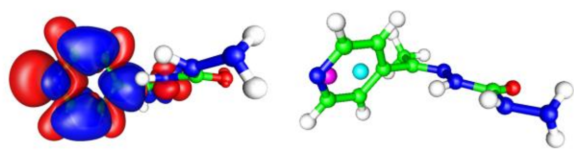

9

Figure. S50. ICT processes in compounds **1-3** and **6-9** in *Z* form; Left images - difference between densities in excited and ground state (red and blue - density increase and decrease upon transition, respectively); Right images - positions of barycenters for charge loss (cyan circle) and charge gain (violet circle) upon transition.

References

Božić, A., Filipović, N.R., Novaković, I., Bjelogrlić, S., Nikolic, J., Drmanic, S., Marinković, A., 2017. Synthesis, antioxidant and antimicrobial activity of carbohydrazones. J. Serbian Chem. Soc. 82, 1–14. doi:10.2298/JSC161220045B

Božić, A., Marinković, A., Bjelogrlić, S., Todorović, T.R., Cvijetić, I.N., Novaković, I., Muller, C.D., Filipović, N.R., 2016. Quinoline based mono- and bis-(thio)carbohydrazones: synthesis, anticancer activity in 2D and 3D cancer and cancer stem cell models. RSC Adv. 6, 104763–104781. doi:10.1039/C6RA23940D

, J., 2009. Toward a Generalized Treatment of the Solvent Effect Based on Four Empirical Scales: Dipolarity (SdP, a New Scale), Polarizability (SP), Acidity (SA), and Basicity (SB) of the Medium. J. Phys. Chem. B 113, 5951–5960. doi:10.1021/jp8095727

Chapman, N.B., Shorter, J. (Eds.), 1978. Correlation Analysis in Chemistry. Springer US, Boston, MA. doi:10.1007/978-1-4615-8831-3

Craik, D.J., Brownlee, R.T.C., n.d. Substituent Effects on Chemical Shifts in the Sidechains of Aromatic Systems, in: Progress in Physical Organic Chemistry. John Wiley & Sons, Inc., Hoboken, NJ, USA, pp. 1–73. doi:10.1002/9780470171936.ch1

Farrugia, L.J., 1997. ORTEP -3 for Windows - a version of ORTEP -III with a Graphical User Interface (GUI). J. Appl. Crystallogr. 30, 565–566. doi:10.1107/S0021889897003117

Hansch, C., Leo, A., Hoekman, D., 1995. Exploring QSAR: Hydrophobic, Electronic, and Steric Constants. Explor. QSAR Hydrophobic, Electron. Steric Constants. doi:0.1021/jm950902o

Kamlet, M.J., Abboud, J.L.M., Abraham, M.H., Taft, R.W., 1983. Linear solvation energy relationships. 23. A comprehensive collection of the solvatochromic parameters, .pi.*, .alpha., and .beta., and some methods for simplifying the generalized solvatochromic equation. J. Org. Chem. 48, 2877–2887. doi:10.1021/jo00165a018

Marcus, Y., 1993. The properties of organic liquids that are relevant to their use as solvating solvents. Chem. Soc. Rev. 22, 409. doi:10.1039/cs9932200409

Okawara, T., Imai, K., Ochiai, T., 2006. Free radical scavenger containing semicarbazide derivatives. WO/2006/093124.

Rančić, M.P., Trišović, N.P., Milčić, M.K., Ajaj, I.A., Marinković, A.D., 2013. Experimental and theoretical study of substituent effect on 13C NMR chemical shifts of 5-arylidene-2,4-thiazolidinediones. J. Mol. Struct. 1049, 59–68. doi:10.1016/j.molstruc.2013.06.027

Reynolds, W.F., Gomes, A., Maron, A., MacIntyre, D.W., Tanin, A., Hamer, G.K., Peat, I.R., 1983. Substituent-induced chemical shifts in 3- and 4-substituted styrenes: definition of substituent constants and determination of mechanisms of transmission of substituent effects by iterative multiple linear regression. Can. J. Chem. 61, 2376–2384. doi:10.1139/v83-412